Faraday Discussions

Accepted Manuscript

This manuscript will be presented and discussed at a forthcoming Faraday Discussion meeting. All delegates can contribute to the discussion which will be included in the final volume.

Register now to attend! Full details of all upcoming meetings: http://rsc.li/fd-upcoming-meetings

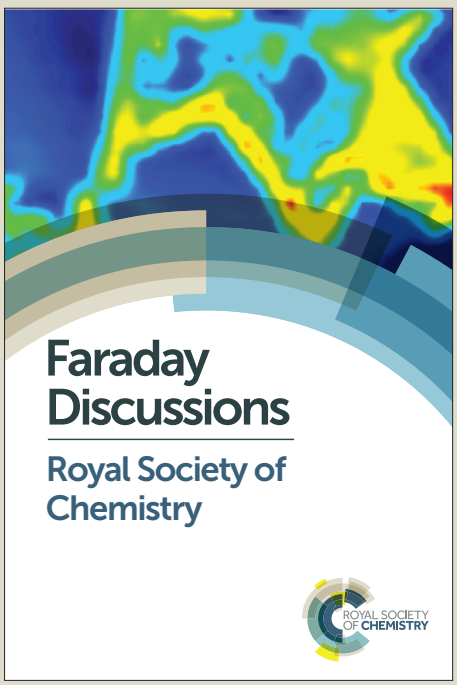

This is an *Accepted Manuscript*, which has been through the Royal Society of Chemistry peer review process and has been accepted for publication.

Accepted Manuscripts are published online shortly after acceptance, before technical editing, formatting and proof reading. Using this free service, authors can make their results available to the community, in citable form, before we publish the edited article. We will replace this *Accepted Manuscript* with the edited and formatted *Advance Article* as soon as it is available.

You can find more information about *Accepted Manuscripts* in the Information for Authors.

Please note that technical editing may introduce minor changes to the text and/or graphics, which may alter content. The journal's standard Terms & Conditions and the Ethical guidelines still apply. In no event shall the Royal Society of Chemistry be held responsible for any errors or omissions in this *Accepted Manuscript* or any consequences arising from the use of any information it contains.

ROYAL SOCIETY OF CHEMISTRY

www.rsc.org/faraday_d

Faraday Discussions

RSCPublishing

ARTICLE

Design of donor-acceptor star-shaped oligomers for efficient solution-processible organic photovoltaics

Cite this: DOI: 10.1039/x0xx00000x

S.A. Ponomarenko[a,b], Y. N. Luponosov[a], J. Min[c], A.N. Solodukhin[a], N.M. Surin[a], M.A. Shcherbina[a], S. N. Chvalun[a], T. Ameri[c], and C. Brabec[c]

Received 30th June 2014,
Accepted 00th June 2014

DOI: 10.1039/x0xx00000x

www.rsc.org/

This contribution describes recent progress in design, synthesis and properties of solution-processible star-shaped oligomers and their application in organic photovoltaics. Albeit different chemistry have been used to design such oligomers, it looks like the most successful approach is based on triphenylamine donor branching center, (oligo)thiophene conjugated spacers and dicyanovinyl acceptor groups. These are mainly amorphous low band-gap organic semiconductors, albeit crystalline or liquid crystalline ordering sometimes can be realized. It was shown that solubility, thermal behavior and structure of such molecules in the bulk strongly depend on the presence and position of alkyl groups, as well as on their length. Photovoltaic properties of solution-processed molecules of this type now approaching 5% that exceed those of vacuum-sublimed devices. Design rules and future perspectives of this class of organic photovoltaic molecules are discussed.

Introduction

Organic photovoltaics is a fast growing area of science and technology due to possibility to create light weight large area flexible solar cells, which can be produced by low cost printing or roll-to-roll techniques.[1] It is based on organic semiconductors, either π-conjugated polymers[2] or small molecules[3], capable to efficient light absorption in the visible spectral range with creation of excitons. However, as opposite to inorganic solar cells, charge separation in organic solar cells (OSC) leading to a photovoltaic effect takes place on the interface between the electron donor and the electron acceptor organic semiconductors.[4] In order to maximize this interface area, the so called "bulk heterojunction" OSCs, consisting of a phase-separated mixture of donor and acceptor organic semiconductors were suggested.[5] In the case of solution-processing of organic semiconductors, which is considered to be a cost-effective alternative to expensive high vacuum processing techniques, such bulk heterojunction (BHJ) is formed by a spontaneous phase separation of organic semiconductors during the solvent evaporation.[6] For creation of the most efficient BHJ OSC typical dimensions of the donor and the acceptor phases should be on the order of 10-20 nm that is comparable to the exciton diffusion length. Moreover, these phases have to be highly interconnected to allow electrons and holes separated on their interphase to reach the electrodes and give a photocurrent. That is why morphology of bulk heterojunctions plays a crucial role on the performance of BHJ OSCs.[7] Ability to control the morphology depends first of all on the chemical structure of a particular organic semiconductor, its solubility and compatibility of two types of organic semiconductors used in BHJ.[8] Therefore, design of novel solution-processible organic semiconductors is a main road for creation of highly efficient BHJ OSCs. Further improvements of the morphology and hence the efficiency of BHJ OSCs can be made by inclusion of various additives during solution processing, like 1,8-octanedithiol or 1,8-diiodooctane,[9] or by different post-treatment techniques, like thermal or solvent vapor annealing.[10] Introduction of special interfacial layers into the device structure of OSC, which helps in optimization of the electronic and electrical properties between the interfaces of light-harvesting active layer and charge-collecting electrodes, can further improve their efficiency.[11]

Nowadays it is accepted that theoretical efficiency of BHJ OSCs can reach as high as 10% in single junction structures and 15% in tandem devices.[12] Recent achievements in organic photovoltaic materials design, morphology optimization and device architectures showed fast progress towards these values: power conversion efficiency (PCE) of 7-9% was reported for solution-processed single junction BHJ OSCs[13] and above 10% for tandem structures.[14] It is noteworthy that in all these high efficiency organic photovoltaic devices soluble fullerene derivative $PC_{71}BM$ was used as acceptor and different low bandgap small molecules or polymers served as donor organic semiconductors. Design of the latter is based on the concept of incorporation of different donor and acceptor units in the structure of such oligomeric or polymeric molecule, which allow tuning their HOMO and LUMO levels, leading to a narrow band gap, which means less than 1.9 eV reported for the "standard" organic semiconductor poly(3-hexylthiophene) P3HT, widely used in organic photovoltaics.[15] Albeit the record efficiencies of BHJ OSCs based on small

molecules and polymers are comparable now, a clear advantage of the small molecules is their exact molecular structure, absence of any polydispersity and different chain ends, which leads to less batch to batch variations during their large scale synthesis and easier purification process. Among the small molecules used as donor materials in organic photovoltaics one can distinguish two different classes: linear and star-shaped molecules. The first class is widely investigated, which already led to impressive PCE of the BHJ OSC devices based on them, mentioned above. The star-shaped molecules seems to be less researched and it is worth to consider them in details in this paper based on resent achievements made in our group in order to outline the design rules leading to the most efficient star-shaped molecules for organic photovoltaic devices and future perspective of this class of materials.

Results and discussion

Overview of the literature data on different star-shaped molecules used in organic photovoltaic devices.

The first star-shaped molecule, properties of which were checked in OSCs, was planarized star-shaped oligothiophene **1** reported by Roncali at. al. (Fig. 1).[16] Under a while light illumination at 77 mW/cm^2 irradiation intensity, a bilayer OSCs, prepared by vacuum evaporation of **1** as donor and N,N'-*bis*(tridecyl)perylenedicarboxyimide (DP13) as acceptor, showed open circuit voltage (V_{oc}) of 0.86 V, short circuit current (J_{sc}) of 1.35 mA/cm^2 and fill factor (FF) of 0.51, which gives overall PCE of 0.77%. This value itself was not very high, albeit it was significantly better as compared to a similar device made from its lineal analogue **2**, containing a central core and just a one arm of the star, which under the same conditions showed PCE of 0.04% only. This difference in behaviour was explained by different orientation of the linear and the star-shaped compounds in thin films, supported by X-ray and UV-Vis optical spectroscopy investigations. The linear oligomer **2** has a preferential vertical orientation of the molecules onto the surface of the substrates, while the star-shaped compound **1** has a preferential horizontal orientation, which is more favourable for absorption of the incident light.

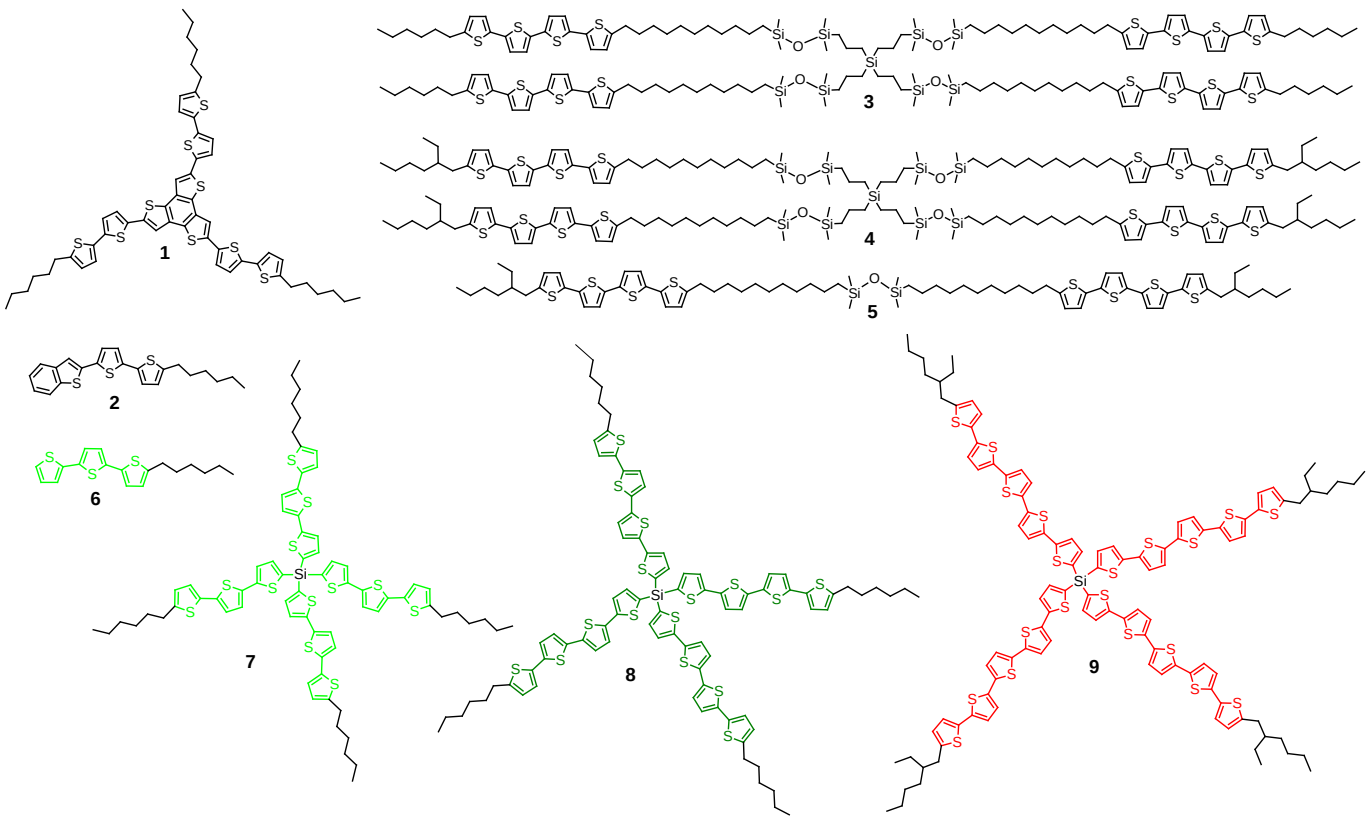

Fig. 1. Chemical structures of star-shaped oligothiophenes and their linear analogues used in organic photovoltaic devices.

Similar conclusions were made after investigation of a series of quaterthiophene-based multipods **3**-**5** with linear and branched terminal alkyl groups (Fig. 1).[17] It was found that multipods with branched 2-ethylhexyl groups **4** and **5** showed better photovoltaic characteristics in solution-processible BHJ OSC, as compared to multipod **3** with linear hexyl groups: PCE = 0.9% and 0.27 vs 0.05% were reported (Table 1).[17b] In all these devices one of the multipods served as a donor and soluble fullerene derivative $PC_{71}BM$ as an acceptor organic semiconductor. Such behaviour was attributed not only to better solubility and improved

morphology of multipods **4** and **5**, but also to a different orientation of their molecules relative to the surface of the substrate: star-shaped multipod **3** with linear end groups tend to have a vertical orientation, while its analogue **4** with branched end groups tend to have more horizontal orientation. It was subsequently confirmed by X-ray analysis, which showed 22 and 55 degrees inclination of the quaterthiophene groups in the multipods **3** and **4**, respectively, in their unit cells.[17c]

Table 1. Photovoltaic characteristics of OSCs prepared from different star-shaped molecules and their linear analogues.

Donor	λ_{max}(abs) in solution/film	Optical band gap, eV	Acceptor	Device type, D:A ratio	I, [a] mW·cm^{-2}	V_{oc}, V	I_{sc}, mA·cm^{-2}	FF, %	PCE, %	Ref.
1	405/420	2.9 (2.55[c])	DP13	bilayer	77	0.86	1.35	51	0.77	16
2*	379/319	3.0	DP13	bilayer	77	0.74	0.094	46	0.04	16
3	403/ - [b]	2.6	$PC_{71}BM$	BHJ, 1:3	100	0.36	0.45	29	0.05	17b
4	403/380	2.6 (2.3[d])	$PC_{71}BM$	BHJ, 1:3	100	0.60	1.3	35	0.27	17b
5	402/399	2.6 (2.3[d])	$PC_{71}BM$	BHJ, 1:3	100	0.68	3.2	40	0.90	17b
6*	367/ -	-	DP13	bilayer	80	0.76	0.14	32	0.04	18
7	384/406	2.65[c]	DP13	bilayer	80	0.99	0.36	42	0.20	18
7a	390/390	2.65[c]	$PC_{61}BM$	BHJ, 1:3	80	0.85	1.13	24	0.29	18
7	385/-	2.85	$PC_{71}BM$	BHJ, 1:2	100	0.83	2.9	25	0.6	19
8	415/-	2.6	$PC_{71}BM$	BHJ, 1:2	100	0.75	5.0	26	1.0	19
9	435/-	2.5	$PC_{71}BM$	BHJ, 1:2	100	0.80	6.0	28	1.4	19

Notes: * linear analogue, [a] AM 1.5 Illumination intensity, [b] no data reported, [c] from thin film measurements, [d] electrochemical bandgap.

Since orientation of the chromophores in the space seems to be very important for the efficiency of photovoltaic devices, the other type of star-shaped molecules – tetrahedral oligothiophenesilanes **7** – **9** seems to be very promising. Under any orientation of such molecule in the space, some the oligothiophene groups orient more or less horizontal to the surface of the cell. This leads to efficient light harvesting in the region of the spectral match of the oligothiophene and the solar light (Table 1). Moreover, non-planar structure of these molecules makes them highly soluble in normal organic solvents like chloroform, toluene, THF, etc. The first oligothiophenesilane **7** was reported by Roncali at. al.[18] Bilayer heterojunction solar cells prepared from **7** as a donor material and DP13 as an acceptor material showed a high V_{oc} of 0.99 V, reasonably good FF of 51%, but low overall PCE of 0.2% mainly due to a low J_{sc} of 0.36 mA/cm^2. However, a clear advantage of the star-shaped structure over its linear analogue, α-hexylterthiophene **6**, was demonstrated: similar device prepared with **6** as a donor showed reduced photovoltaic characteristics with PCE of 0.04% only. In the same work terthiophenesilane **7a**, which has *n*-hexylthiole instead of *n*-hexyl end-capping group, leading to somewhat higher solubility, was reported. In combination with $PC_{61}BM$ acceptor it was used as a donor in solution-processed BHJ OSC device, which showed improved J_{sc} of 1.13 mA/cm^2, but just slightly higher PCE of 0.29% mainly due to a reduced fill factor to 24%.

Our group was able to synthesize soluble oligothiophenesilanes **7** – **9** with different conjugation length ranging from three to five conjugated thiophene rings.[19] Since solubility in this series of star-shaped molecules decreased with increasing the conjugation length, like it usually happens for linear oligothiophenes, it was necessary to use branched 2-ethylhexyl end-capping groups for quinquethiophenesilane **5** to make it soluble. The efficiency of solution-processible BHJ OSCs prepared from compounds **7** – **9** as donor and $PC_{71}BM$ as acceptor improved with increasing the conjugation length: from 0.6% for **7** to 1.4% for **9** (Table 1). A major improvement comes from the short circuit currents, which lay in the range 2.9 - 6.0 mA/cm^2 with a clear tendency to increase for higher conjugation length of the donor, meaning the better efficiency of the light absorption for more conjugated molecules. Interestingly, that the external quantum efficiency (EQE) reaches the values above 20% in a broad wavelength range from 380 to 580 nm for quaterthiophenesilane **8** and above 30% in the region between 400 and 500 nm for quinquethiophenesilane **9**, i.e. in the region of efficient light absorbance of these two donor compounds, with a clear impart of the acceptor absorbance. Further improvements of PCE are possible with donor molecules, having lower bandgap than those of the oligothiophenes considered above.

A fruitful approach to the preparation of low band gap star-shaped molecules is based on the usage of triphenylamine (TPA) donor branching core and different accepting groups located in the arms of these molecules.[20] The first such molecules were reported by Roncali at. al. (**10** and **11** in Fig. 2).[21] They contained α-hexylterthienyl or 3′,4′-ethylenedioxy-5′′-hexyl-5-terthienyl groups, respectively. A bilayer OSC obtained by sin-coating of **10** or **11** donor material followed by vacuum evaporation of C_{60} acceptor showed, however, low PCE, 0.32 and 0.14% respectively (Table 2). BHJ OSC prepared from spin-coating of the mixture of TPA-based donor molecule **12** having three (2-thienylethen-2-yl)-2-thienyl groups and $PC_{61}BM$ acceptor showed similar photovoltaic behaviour with PCE = 0.41%.[22a] Similar TPA-based molecule **13** with pyrenylimide-quaterthienyl arms reported by

Cremer and Bauerle,[23] albeit has significantly lower optical bandgap of 2.01 eV, in BHJ OSCs with $PC_{61}BM$ acceptor showed PCE of 0.25%. In fact, this molecule have several optical transitions, the shortest of which (at 429 nm) can be attributed to the conjugated quaterthiophene-phenylene system, while the longest (at 520 nm) – to intramolecular charge transfer (ICT) from TPA-donor group to a pyrenylimide acceptor group. Similar situation was identified for TPA-molecule **14** with dicyanovinyl (DCN) acceptor groups by Roncali at. al.[22] Initial efforts showed PCE of 1.02% for a bilayer device with **14** as a donor and C_{60} as an acceptor.[22a,b] Further optimization of the device structure allowed to increase its efficiency to PCE=1.85%.[22c] More elongated TPA-DCN molecules with bithienyl (**15**) or bithienylethenyl (**16**) conjugated spacers were reported by Jing Zhang at. al.[24a] BHJ OSCs with **15** or **16** as donors and $PC_{71}BM$ as acceptor showed PCE of 1.4 and 3.0%, respectively. To make them soluble, 3-hexylthienyl instead of thienyl groups were used. Star-shaped oligomer **16** had a remarkable shift of the absorption edge on 78 nm as compared to oligomer **15**, leading to a narrow band gap of 1.65 eV *vs* 1.83 eV (Table 2). Combination of a good solubility (18 g/L) with a narrow band gap of **16** are the most probable factor, which lead to a record PCE in this series of the star-shaped oligomers. Comparable results were obtained by the same group for TPA star-shaped molecule **17** with thieno[3,2-b]thiophene–dicyanovinyl arms.[24b] BHJ OCS with **17** as donor and $PC_{61}BM$ as acceptor showed PCE of 1.63%. Replacing $PC_{61}BM$ by $PC_{71}BM$ led to increasing in PCE to 2.87% due to a wider absorption spectra of $PC_{71}BM$. Good solubility of **1**7 were governed by the presence of two hexyl groups at each thieno[3,2-b]thiophene unit.

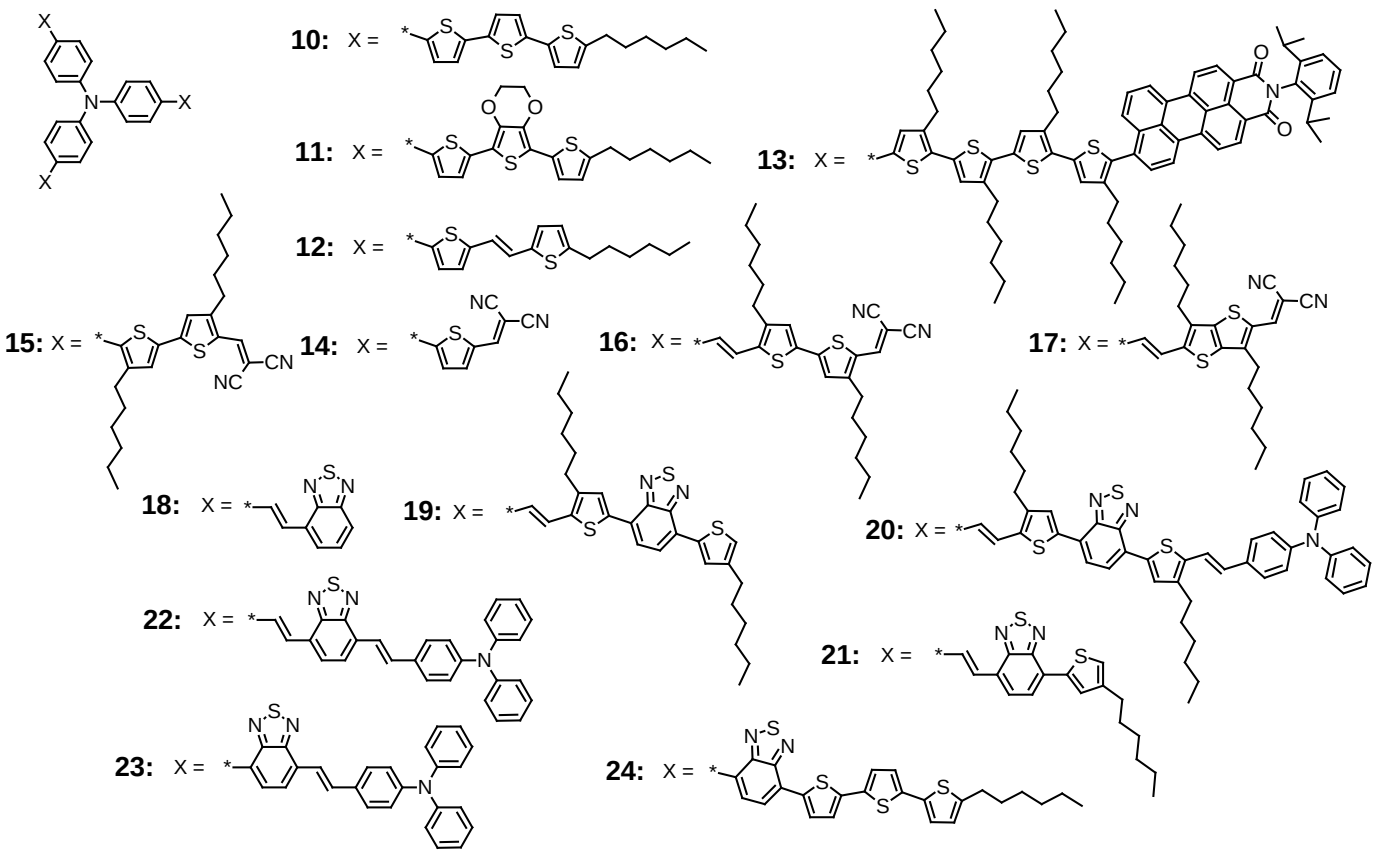

Fig. 2. Chemical structures of triphenylamine-based star-shaped molecules used in organic photovoltaic devices.

One of the other strong donor groups is benzothiadiazole, which was also used for design of TPA-based donor-acceptor molecules. Yongfang Li group reported the synthesis of such star-shaped molecule **18** with benzo[1,2,5]thiadiazolvinylene arms.[25a] Its 1:3 mixture with $PC_{61}BM$ led to BHJ OSC with a PCE of 0.61%. Elongation of these arms with two 3-hexylthienyl units (**19**) and further with ethynyltriphenylene (**20**) units led to lowering of the band gap from 2.04 to 1.88 and 1.76 eV, respectively (Table 2).[25b] BHJ OSCs prepared from **19** or **20** with $PC_{71}BM$ acceptor led to improved PCE of 1.90 and 1.23%, respectively. Attaching just a 3-hexylthyenyl unit to **18** led to molecule **21**, which in the mixture with $PC_{71}BM$ acceptor showed photovoltaic efficiency of 2.39%.[25c] Alternative elongation of benzo[1,2,5]thiadiazolvinylene arms with ethylene-triphenylamine group (**22**) led to BHJ OSC with PCE of 1.33% using $PC_{61}BM$ acceptor and with PCE of 3.37% using $PC_{71}BM$ acceptor.[25d,e] Direct linking of benzothiazole-ethylene-triphenylamine arm to a TPA core in star-shaped molecule **23** allowed to measure PCE of 3.14%, using $PC_{71}BM$ acceptor.[25f] Interestingly that simple incorporation of benzothiazole unit between TPA core and α-

hexylterthiophene arm in **24** allowed further improvement of photovoltaic properties in BHJ OSC: to PCE = 2.34% using $PC_{61}BM$ acceptor and to PCE=4.3% using $PC_{71}BM$ acceptor.[25g]

Table 2. Photovoltaic characteristics of OSCs prepared from triphenylamine-based star-shaped molecules.

Donor	λ_{max}(abs) in solution/film	Bandgap, eV	HOMO/LUMO, eV	Acceptor	Device type, D:A ratio	V_{oc}, V	I_{sc}, mA·cm^{-2}	FF, %	PCE,[a] %	Ref.
10	429/440	2.55 (2.4[c])	-5.24[e] / -[b]	C_{60}	bilayer	0.67	1.7	30	0.32	21
11	439/450	2.50 (2.4[c])	-5.18[e] / -	C_{60}	bilayer	0.32	1.5	30	0.14	21
12	424/435	2.38	-5.33[e] / -	$PC_{61}BM$	BHJ, 1:3	0.60	2.43	28	0.41	22a
13	429,495,**520**/ 446,490,**515**	2.01 (1.48[d])	-5.04[e] / -3.36[e]	$PC_{61}BM$	BHJ, 1:4	0.60	1.4	29	0.25	23
14	368,**509**/ 382,**538**	1.78	-5.48[e] / -	C_{60} C_{60}	bilayer bilayer	0.96 1.15	3.65 4.59	29 28	1.02 1.85[f]	22a,d 22c
15	296,342,**504**/ 312,402,**563**	1.83[c] (1.88[d])	-5.22 / -3.34	$PC_{71}BM$	BHJ, 1:2	0.84	5.21	30.8	1.4	24a
16	298,357,**518**/ 320,421,**585**	1.65[c] (1.61[d])	-5.03 / -3.42	$PC_{71}BM$	BHJ, 1:2	0.88	7.76	43.9	3.0	24a
17	429,**542**/ 432,**580**	1.77[c]	-5.13 / -3.38	$PC_{61}BM$ $PC_{71}BM$	BHJ, 1:2 BHJ, 1:2	0.9 0.96	4.66 6.80	38.8 43.5	1.63 2.87	24b 24b
18	320,341,460/ 324,351,486	2.14 (2.04)[d]	-5.41 / -3.37	$PC_{61}BM$	BHJ, 1:3	0.89	1.66	0.41	0.61	25a
19	402,544/ 414,552	1.88	-5.30 / -3.42	$PC_{71}BM$	BHJ, 1:3	0.75	6.41	39.0	1.90	25b
20	410,560/ 416,576	1.76	-5.14 / -3.38	$PC_{71}BM$	BHJ, 1:3	0.71	5.41	32.0	1.23	25b
21	316,361,509/ 320,370,529	1.96 (2.11)[d]	-5.19 / -3.08	$PC_{71}BM$	BHJ, 1:3	0.85	8.58	32.7	2.39	25c
22	375,531/ 541	1.86	-5.3 / -3.27	$PC_{61}BM$ $PC_{71}BM$	BHJ, 1:3 BHJ, 1:3	0.81 0.84	4.18 9.10	39.0 44.1	1.33 3.37	25d 25e
23	328,501/ 327,509	2.05	-5.15 / -2.99	$PC_{71}BM$	BHJ, 1:3	0.92	7.77	44.0	3.14	25e,f
24	328,380,512/ 338,390,**538**	1.9	-5.28 / -3.11	$PC_{61}BM$ $PC_{71}BM$	BHJ, 1:3 BHJ, 1:2	0.86 0.87	5.90 9.51	46.2 52	2.34 4.3	25g 25g

Notes: [a] measured at AM 1.5 G under Illumination intensity of 100 mW/cm^2, unless otherwise stated; [b] no data reported, [c] estimated from the edge of the thin film absorption spectra, [d] measured electrochemically; [e] estimated in this paper from the CVA data given in the reference; [f] measured at AM 1.5 G under Illumination intensity of 80 mW/cm^2.

Thus, nowadays there is quite a lot of different TPA-based star-shaped molecules used in organic photovoltaics applications, the most efficient of which includes strong dicyanovinyl or benzothiadiazole units. However, any systematic investigations of the influence of their molecular structure on their photovoltaic performance have not been yet reported. Moreover, photovoltaic properties of different molecules were measured in different device architectures, with different acceptors or donor:acceptor ratios, that does not allow their direct comparison. Below we compare a series of TPA-based star-shaped molecules with different conjugation length and solubilizing alkyl chain ends **N(TPA-nT-DCN-Alk)$_3$** with the molecule without alkyl groups **N(TPA-2T-DCN)$_3$** (Fig. 3). Their optical, electrochemical, photovoltaic and thermal properties, as well as structure in the bulk, measured under identical conditions, should allow elucidating the design rules of the most efficient structures of star-shaped molecules for organic photovoltaic applications.

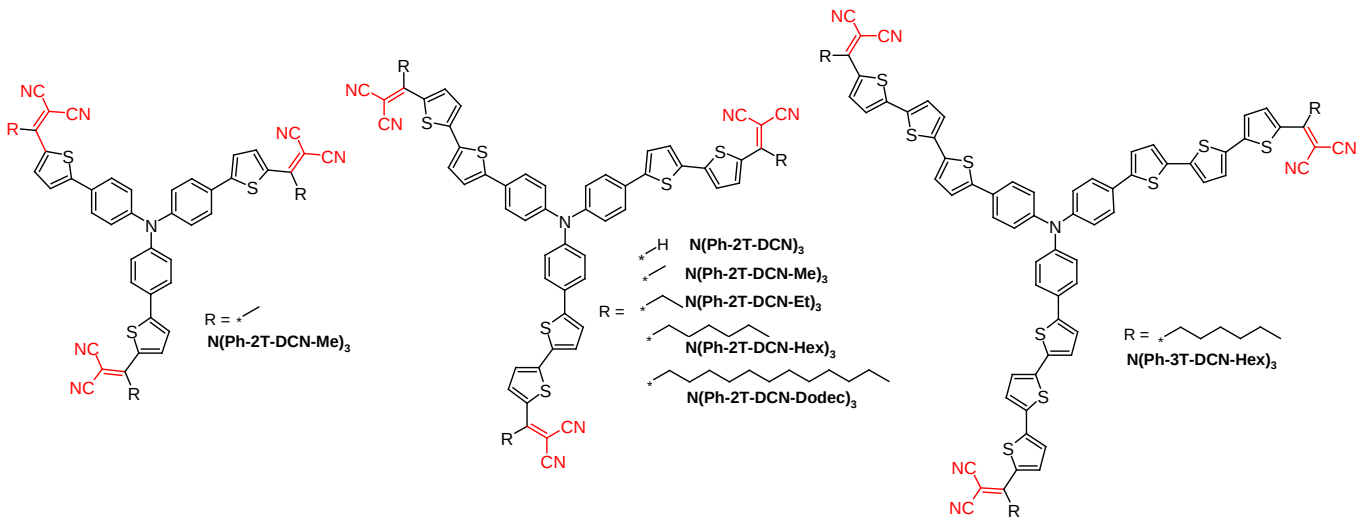

Fig. 3. Chemical structures of TPA-based star-shaped molecules with different conjugation length and both without alkyl groups **N(TPA-2T-DCN)$_3$** and with solubilizing alkyl chain ends **N(TPA-nT-DCN-Alk)$_3$**.

Synthesis of star-shaped molecules with triphenylamine donor core and dicyanovinyl acceptor arms.

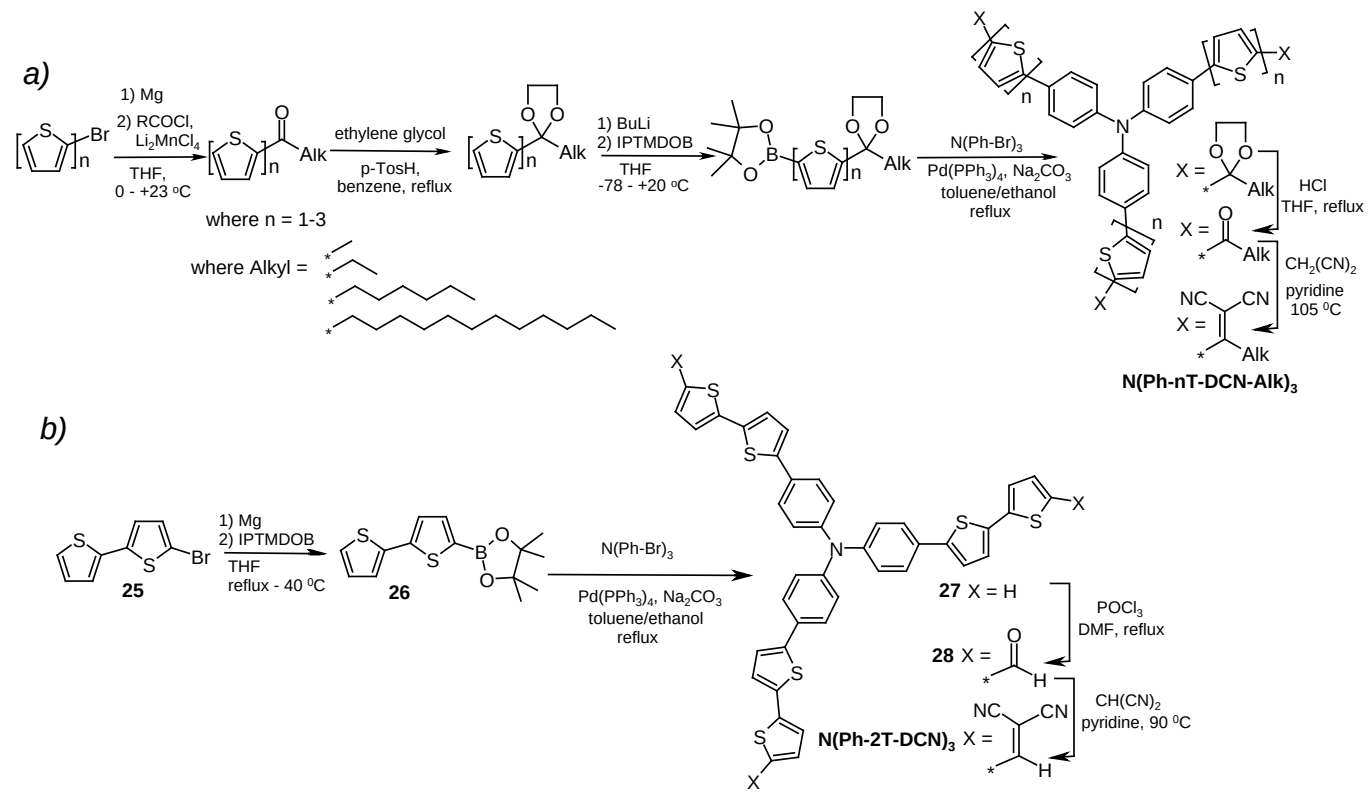

Fig. 4. Scheme of synthesis of TPA-based star-shaped molecules with (a) and without (b) alkyl groups.

Chemical structures of all TPA-based star-shaped molecules under consideration are presented in Figure 3. A general scheme of synthesis of the molecules with terminal alkyl chains **N(TPA-nT-DCN-Alk)$_3$** is outlined in Figure 4a. Their preparation consists of six steps.[26] The first step includes preparation of oligothienyl ketones with different number of conjugated thiophene rings by acylation of the magnesium derivatives of oligothienyl bromides with corresponding alkanoyl chlorides. The second step requires preparation of the protected ketones in order to use them on the third stage of the reaction, which includes formation of their lithium derivatives followed by the reaction with 2-isopropoxy-4,4,5,5-tetramethyl-1,3,2-dioxaborolane (IPTMDOB) for the preparation of pinacol boronic esters. On the fourth step Suzuki cross-coupling reaction between the organoboron compounds prepared and *tris*(4-bromophenyl)amine is carried out to obtain the star-shaped precursors with protected ketone groups. Then

simple treatment of their solutions in THF with hydrochloric acid at reflux led to precipitation of poorly soluble star-shaped ketones in high yields (95-99%). Successful substitution of three carbonyl groups with dicyanovinyl functions required to elaborate and to optimize the conditions of Knövenagel condensation. As a result, all TPA-based molecules **N(TPA-nT-DCN-Alk)$_3$** were synthesized in high reaction yield (90-95%) via Knövenagel condensation between trifunctional ketones and an excess of malononitrile under a microwave heating, using pyridine both as a base and as a solvent. Microwave heating at the last reaction step was found to decrease both the reaction time and the amount of by-products as compared to conventional heating.

Synthesis of the star-shaped molecule without alkyl groups **N(TPA-2T-DCN)$_3$** was carried out in four steps using the synthetic approach developed earlier by Roncali et. al. for similar molecules[22] (Fig. 4b). It should be noted, however, that synthesis of the same molecule via a scheme of protection/deprotection of carbonyl groups was done recently in 5 steps with 37 % overall yield starting from 2,2'-bithiophene-5-carbaldehyde.[22b] In this work it was obtained in 52% overall yield by an alternative technique. On the first step 2-(2,2'-bithien-5-yl)-4,4,5,5-tetramethyl-1,3,2-dioxaborolane (**26**) was synthesized by the reaction between IPTMDOB and 2′-bithien-5-yl magnesium bromide, prepared *in situ* from 5-bromo-2,2′-bithiophene (**25**) and magnesium, in 97% isolated yield. A Suzuki cross-coupling between **26** and *tris*(4-bromophenyl)amine gave star-shaped precursor **27** in 90% yield. Vilsmeier-Haack formylation of compound **27** led to *tris*[4-(5-formyl-2,2'-bithiyenyl]amine **28** in 90% yield. Finally, **N(Ph-2T-DCN)$_3$** was obtained in 60 % isolated yield by Knövenagel condensation reaction of compound **28** with an excess of malononitrile in pyridine under a microwave heating. The purity and molecular structure of all precursors and final molecule was proved by ^{1}H-, and IR, spectroscopy, elemental analysis, and MALDI-TOF (see Experimental part and Supporting Information, Fig. S1 - S4).

Optical and electrochemical properties of star-shaped molecules with triphenylamine donor core and dicyanovinyl acceptor arms.

Optical properties of the seven TPA-DCN molecules synthesized were investigated both in dilute solutions and in thin films. Fig. 5 shows the UV-vis absorption spectra of dilute solutions of these star-shaped small molecules in *o*-dichlorobenzene (ODCB) and thin films doctor bladed on quartz substrates. The corresponding optical data are summarized in Table 3. It should be noted that all these compounds are soluble in polar organic solvents, like THF, chloroform, ODCB, etc. Estimation of their solubility was made by dissolving the compounds in ODCB (1 mL) until relevant molecules remained undissolved at room temperature and filtering the complete solution obtained through a 0.25-μm PTFE syringe filter. Immediately after filtration the solution was quickly and quantitatively transferred (500 μL) into another glass bottle of known mass, the solvent from the filtrate was evaporated and the residue was weighted. After that solubility of the relevant material was calculates. It was found that solubility decreases with elongation of the arm conjugation length, when going from 1T to 2T and 3T-contining molecules, but it significantly improves with increasing the alkyl chain length or even adding methyl groups to the DCN groups. As a result, a reasonable compromise between the conjugation length and the alkyl chain end can be found to realize solution-processable star-shaped molecules.

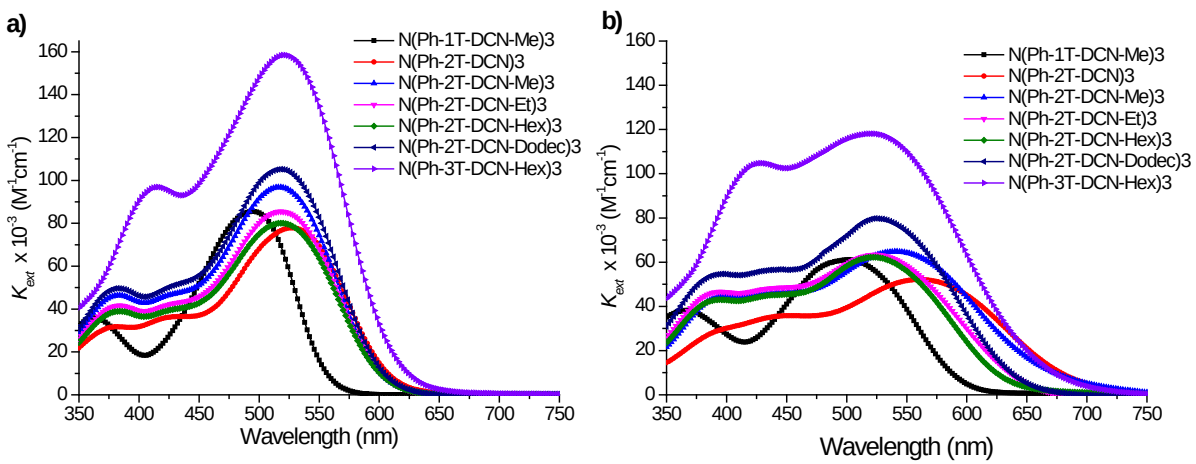

Fig. 5. Absorption spectra of TPA-DCN star-shaped molecules in ODCB solution (a) and in the film (b) shown as distribution of their molar extinction coefficients K_{ext}.

Onsets of the absorption spectra of these molecules in solution (Fig. 5a) are clearly grouping in three cases, corresponding to different conjugation lengths of the arms of the molecules: 1) at 560 nm for 1T-containing molecule **N(Ph-1T-DCN-Me)$_3$**, 2) at ca. 603 nm for 2T-containing molecules **N(Ph-2T-DCN-Alk)$_3$** and 3) at 615 nm for 3T-containing molecule **N(Ph-3T-DCN-Hex)$_3$**. Absorption edge of 2T-containing molecule without alkyl ends **N(Ph-2T-DCN)$_3$** lies at 611 nm, that is in between the

second and the third cases, indicating a small influence of alkyl substituents at dicyanovinyl groups on the optical properties. The absorption spectra of the five 2T-containing molecules in solutions show similar absorption peaks and regions, exhibiting strong visible absorption peaks at ca. 382 nm (with molar extinction coefficients K_{ext} = 31 700 – 49 600 $M^{-1}cm^{-1}$) and ca. 517 nm (with 2 – 2.5 times higher K_{ext} = 77 800 – 105 000 $M^{-1}cm^{-1}$), as can be seen on Fig. 5a. The absorption peak at 382 nm in the short wavelength region corresponds to the π-π* transition. And the visible absorption peak at 517 nm can be attributed to the intramolecular charge-transfer (ICT) transition between the triphenylamine (TPA)-2T donor unit and the dicyanovinyl (DCN) acceptor unit. As compared to the five 2T-containing molecules, the absorption peaks of the 1T-containing **N(Ph-1T-DCN-Me)$_3$** are blue-shifted significantly to 363 nm and 495 nm. Their molar extinction coefficients are 35 800 $M^{-1}cm^{-1}$ and 85 500 $M^{-1}cm^{-1}$, respectively. Probably, the shorter oligothiophene π-bridges linkage between TPA and DCN increase torsional interactions and reduce the strength of the ICT transition, which determines the bandgap of the molecules under consideration. The optical bandgaps of the 2T-containing molecules **N(Ph-2T-DCN-Alk)$_3$** in solution are 2.05 – 2.06 eV, it is somewhat smaller (2.03 eV) for **N(Ph-2T-DCN)$_3$**, while corresponding bandgap of **N(Ph-1T-DCN-Me)$_3$** is significantly larger, 2.22 eV. Considering these reasons, the shorter wavelength region peaks redshift from 363 nm/382 nm to 416 nm for **N(Ph-3T-DCN-Hex)$_3$**, which is attributed to the stronger localized π-π* transition arising from the longer oligothiophene π-bridge lengths. Peak at 416 nm has a remarkable high K_{ext} = 96 800 $M^{-1}cm^{-1}$, while the ICT transition of this molecule at 522 nm has the highest K_{ext} = 158 000 $M^{-1}cm^{-1}$ in the whole series of molecules under consideration. In addition, the similar absorption peaks for **N(Ph-3T-DCN-Hex)$_3$** in solution comparing with the 2T-contining molecules suggests that the longer oligothiophene π-bridge lengths of star-shaped molecules have not obvious influence on the ICT transition.

Table 3. Optical properties of the TPA-DCN star-shaped molecules in dilute ODCB solutions and thin films.

Compound	Solution [a]					Film [b]			
	Solubility, $g \cdot L^{-1}$	λ_{max}, nm	K_{ext}, M^{-1} cm^{-1}	λ_{onset}, [c] nm	E_g^{opt}, [d] eV	λ_{max}, nm	K_{ext}, M^{-1} cm^{-1}	λ_{onset}, [c] nm	E_g^{opt}, [d] eV
N(Ph-1T-DCN-Me)$_3$	6	362 495	35 800 85 500	559	2.22	368 502	38 200 61 100	596	2.08
N(Ph-2T-DCN)$_3$	2	382 528	31 700 77 800	611	2.03	392 560	28 800 52 100	698	1.78
N(Ph-2T-DCN-Me)$_3$	3	384 517	46 300 96 800	602	2.06	400 541	44 800 64 700	690	1.80
N(Ph-2T-DCN-Et)$_3$	8	384 517	41 700 85 500	604	2.05	394 525	46 600 63 400	646	1.92
N(Ph-2T-DCN-Hex)$_3$	20	384 517	39 000 80 100	604	2.05	394 525	43 000 62 200	636	1.95
N(Ph-2T-DCN-Dodec)$_3$	52	382 517	49 600 105 000	603	2.06	396 525	54 700 79 700	641	1.93
N(Ph-3T-DCN-Hex)$_3$	12	416 522	96 800 158 000	615	2.02	428 522	105 000 118 000	668	1.85

[a] Measured in ODCB solution. [b] Cast from ODCB solution. [c] Estimated as a wavelength at which the absorption decreases to 10% from its maximum value. [d] Bandgap estimated from the onset wavelength (λ_{onset}) of the optical absorption: E_g^{opt} = 1240/ λ_{onset}.

Comparative analysis of solution and thin films' photophysical properties revealed that absorption spectra of these molecules become broader and their absorption peaks are significantly red-shifted, as shown in Fig. 5b and Table 3. Broadening the absorption peaks is accompanied by decreasing their absorption coefficients, especially of their long wavelength ICT transitions (at 502 – 560 nm) – they decreases in 1.3 – 1.5 times. However, changes in their short wavelength π-π* transitions are much smaller: their molar extinction coefficients K_{ext} changes just on 10%, and these changes can have either direction (increasing or decreasing of K_{ext}). Such changes in the K_{ext} make the absorption of these molecules in thin film more smoothly distributed through the whole absorption spectra as compared to their solution. The most significant changes can be seen for onsets of the absorption spectra of these molecules in films (Fig. 5b). As in the case of solutions, they can also be grouped in three cases, albeit somewhat different than those in the solutions: 1) at ca. 600 nm for 1T-containing molecule **N(Ph-1T-DCN-Me)$_3$**, 2) at ca. 630 - 650 nm for 2T-containing molecules **N(Ph-2T-DCN-Alk)$_3$** with ethyl, hexyl and decyl groups and 3) at ca. 670 – 700 nm for 2T-containing molecules **N(Ph-2T-DCN)$_3$** and **N(Ph-2T-DCN-Me)$_3$**, as well as for 3T-containing molecule **N(Ph-3T-DCN-Hex)$_3$**. The absorption spectra of **N(Ph-2T-DCN)$_3$** is broader than those of **N(Ph-2T-DCN-Me)$_3$**, and even more than these of the other three 2T-containing molecules with the longer alkyl terminal chains. These results indicate that there are strong intermolecular interactions leading to aggregation in the **N(Ph-2T-DCN)$_3$** and **N(Ph-2T-DCN-Me)$_3$** film. It is likely that the long alkyl terminal chains could increase steric hindrance and torsional interactions between the DCN groups and 2T-bridges and shorten the

conjugated length of each branch in the molecule. Interestingly, the absorption peak of **N(Ph-3T-DCN-Hex)$_3$** is negligibly shifted between solution and film. It may be attributed to the weak aggregation and intermolecular interactions of the molecules in the solid state. In addition, due to the decreased branch conjugation length and poor electronic communication between TPA and DCN units, 1T-containing **N(Ph-1T-DCN-Me)$_3$** exhibit a high solid state optical band gap of 2.08 eV, while it is significantly lower (1.80 eV) for its 2T-homologue **N(Ph-2T-DCN-Me)$_3$** and 1.78 eV for 2T-containing star without alkyl groups **N(Ph-2T-DCN-Me)$_3$**. The other 2T-containing molecules with longer alkyl groups has somewhat larger optical band gaps of 1.92 – 1.95 eV in the solid state due to weaker interactions between the molecules. Finally, compared to the **N(Ph-2T-DCN-Hex)$_3$**, the absorption intensity of **N(Ph-3T-DCN-Hex)$_3$** in the shorter wavelength region is higher, illustrating that longer oligothiophene π-bridge effectively releases the distortion induced by the hexyl terminal chains. Higher conjugation of the arms in **N(Ph-2T-DCN-Hex)$_3$** leads to a rather low optical band gap in the solid state (1.85 eV). It is noteworthy that optical bandgaps in the solid state are ca. 0.10 – 0.26 eV smaller than those in the solution, indicating on different aggregation of the molecules in the solid state.

The electrochemical properties of seven star-shaped molecules under consideration and their highest occupied molecular orbital (HOMO) and lowest unoccupied molecular orbital (LUMO) energy levels were examined by cyclic voltammetry (CVA). From the values of the standard formal reduction potentials (φ_{red}) and the standard formal oxidation potentials (φ_{ox}), the HOMO and LUMO energy levels of these compounds were calculated as presented in Table 3, according to the equations of LUMO = -e(φ_{red}+ 4.40) (eV) and HOMO = -e(φ_{ox} + 4.40) (eV).[27] The results revealed that the measured LUMO energy levels of these seven molecules are very close, suggesting that the incorporation of various oligothiophene π-bridges and alkyl terminal chains has little effect on their LUMO level differences. However, it is interesting to note that the HOMO energy levels are significantly different due to the effect of π-conjugated bridges with various electron donating characters.[28] Owing to the strong electron-donating terthiophene units as π-bridges, **N(Ph-3T-DCN-Hex)$_3$** exhibits a high HOMO energy level of -5.26 eV. And it is 0.34 eV higher than that of **N(Ph-1T-DCN-Hex)$_3$** (-5.60 eV) because of its relatively weak electron-donating thiophene bridges. In addition, the HOMO energy levels of other four 2T-bridge based molecules with various alkyl terminal chains are in between the HOMO energy levels of **N(Ph-1T-DCN-Me)$_3$** and **N(Ph-3T-DCN-Hex)$_3$** and similar, as shown in Table 4.

Table 4. Electrochemical properties of the TPA-DCN star-shaped molecules.

Compound	Cyclic voltammetry data			Energy levels	
	φ_{ox}, V	φ_{red}, V	E_g^{EC}, eV	HOMO, eV	LUMO, eV
N(Ph-1T-DCN-Me)$_3$	1.20	-0.94	2.14	-5.60	-3.46
N(Ph-2T-DCN)$_3$	0.77	- [a]	-	-5.17	-3.39 [b]
N(Ph-2T-DCN-Me)$_3$	0.92	-0.99	1.91	-5.32	-3.41
N(Ph-2T-DCN-Et)$_3$	0.92	-1.00	1.92	-5.32	-3.40
N(Ph-2T-DCN-Hex)$_3$	0.94	-0.99	1.93	-5.34	-3.41
N(Ph-2T-DCN-Dodec)$_3$	0.94	-1.00	1.94	-5.34	-3.40
N(Ph-3T-DCN-Hex)$_3$	0.86	-1.00	1.86	-5.26	-3.40

Notes: φ_{ox} – standard formal reduction potential, φ_{red} – standard formal oxidation potential, E_g^{EC} – electical energy gap. [a] No reversible reduction can be observed. [b] Estimated as a difference between HOMO energy level and optical band gap in thin film.

It should be noted that only HOMO energy level of **N(Ph-2T-DCN)$_3$** can be estimated from the CVA measurements, since this compound shows a reversible formal oxidation potential at +0.77V, but irreversible reduction. This gives the value of HOMO of this compound at -5.17 eV – the highest in the series of compounds under consideration. It is 0.15 eV higher as those for its methyl analogue **N(Ph-2T-DCN-Me)$_3$**, indicting less oxidation stability of the former, which can be attributed to easy oxidation of the liable proton at the dicyanovinyl groups. Similar trend can be observed, when comparing HOMO energy levels of **N(Ph-1T-DCN)$_3$** (compound **14** in Table 2) and **N(Ph-1T-DCN-Me)$_3$**, which were estimated to be -5.48 and 5.60 eV, respectively, giving a difference of 0.12 eV. Moreover, for all alkyl-substituted stars **N(Ph-nT-DCN-Alk)$_3$** both oxidation and reduction potentials are reversible, while the reduction of their proton-containing analogs **N(Ph-1T-DCN)$_3$** and **N(Ph-2T-DCN)$_3$** was found to be irreversible not only in this work, but also in the literature.[22d] Thus, the presence of alkyl substituents at dicyanovonyl groups makes **N(Ph-nT-DCN-Alk)$_3$** stars not only more oxidation stable, but also make reversible their reduction due to stabilization of

anion-radicals by alkyl groups, that can positively influence on the stability of organic photovoltaic devices made from these compounds.

Thermal properties and structure of star-shaped molecules with triphenylamine donor core and dicyanovinyl acceptor arms.

Thermal stability, phase behaviour and structure of the series of TPA-DCN star-shaped molecules were investigated by TGA, DSC, and X-ray diffraction in small and wide angles (WAXS and SAXS). The results obtained are summarized in Table 5. TGA data (See Table 5 and Fig. S5) indicate that all these compounds are thermally stable and demonstrate temperature of 5% decomposition (T_d) above 370 °C both in the inert atmosphere (under nitrogen) and under normal conditions (in the presence of oxygen and water vapours). Temperature of decomposition T_d is diminished with increasing alkyl chain length, which could be explained by the decomposition of the aliphatic tails.

Table 5. Thermal properties of the TPA-DCN star-shaped molecules.

Compound	T_g, °C	ΔC_p, $J \cdot g^{-1}K^{-1}$	T_m, °C	ΔH, $J \cdot g^{-1}$	Phase1	T1, °C	Phase2	T2, °C	Phase 3	T_d (air), °C	T_d (N_2), °C
N(Ph-1T-DCN-Me)$_3$	128	0.27	276	81.8	Crystal	128	Crystal	290	Iso [a]	401	402
N(Ph-2T-DCN)$_3$	146	0.29	276	27.8	Crystal	140	Crystal	276	Iso	405	405
N(Ph-2T-DCN-Me)$_3$	159	0.21	247	60.7	Amorphous Crystal	247	Iso			416	416
N(Ph-2T-DCN-Et)$_3$	114	0.24	-	-	Amorphous					392	402
N(Ph-2T-DCN-Hex)$_3$	64	0.25	-	-	Amorphous					371	403
N(Ph-2T-DCN-Dodec)$_3$	31	0.26	-	-	Col [b]	100	Iso			370	402
N(Ph-3T-DCN-Hex)$_3$	72	0.29	-	-	Col	160	Iso			388	388

Notes: T_g – glass transition, ΔC_p – heat capacity change at the glass transition, T_m – melting temperature, ΔH – melting enthalpy.
[a] Isotropization temperature. [b] Col – Columnar mesophase; T_d - decomposition temperature (at 5% weight-loss).

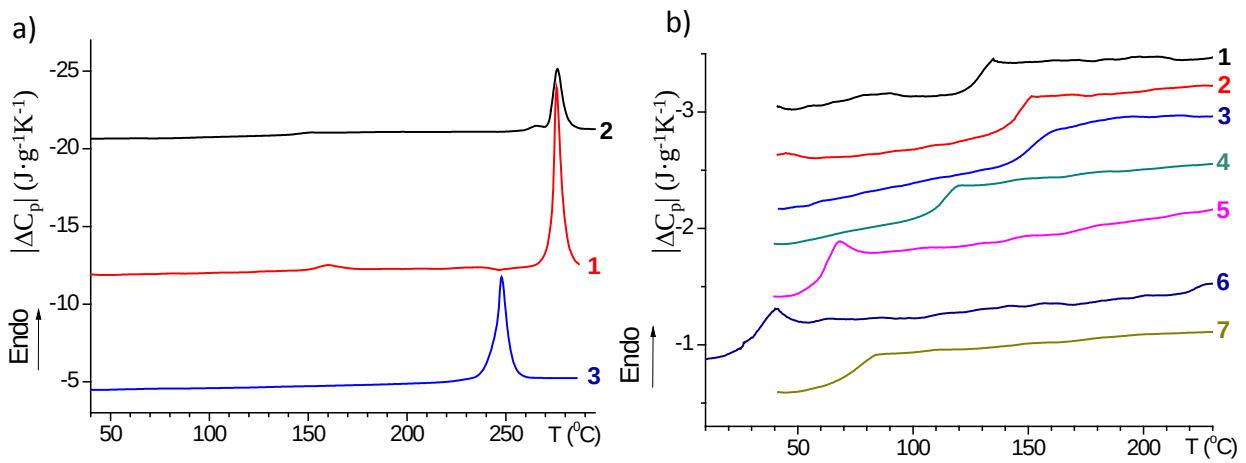

Fig. 6. DSC scans of the first (a) and the second (b) heating of 1) **N(Ph-1T-DCN-Me)$_3$**, 2) **N(Ph-2T-DCN)$_3$**, 3) crystalline fraction of **N(Ph-2T-DCN-Me)$_3$**, 4) **N(Ph-2T-DCN-Et)$_3$**, 5) **N(Ph-2T-DCN-Hex)$_3$**, 6) **N(Ph-2T-DCN-Dodec)$_3$**, 7) **N(Ph-3T-DCN-Hex)$_3$**. For the sake of simplicity, scans are shifted along the heat capacity axis.

DSC analysis revealed that both methyl-containing molecules **N(Ph-1T-DCN-Me)$_3$** and **N(Ph-2T-DCN-Me)$_3$** as well as those without alkyl groups **N(Ph-2T-DCN)$_3$** can be crystalline at the first heating, but their become amorphous after melting, as can be seen on the cooling and the second heating scans (Fig. 6). Such behaviour was used for simplification of the dissolution of these

molecules, since amorphous phases dissolve much faster and easier than the crystalline ones. Interestingly, that melting temperatures of **N(Ph-1T-DCN-Me)$_3$** and **N(Ph-2T-DCN)$_3$** are the same, 276 °C, but their melting enthalpies differ more than three times: 81.1 vs 27.8 J·g^{-1}. However, it should be noted that the latter compound is only partly crystalline and shows both glass transition and melting peak on the same first heating DSC curve. This can be explained by its low solubility, leading to a fast solidification during the solvent evaporation. Both melting temperature and enthalpy of **N(Ph-2T-DCN-Me)$_3$** are lower as compared to its 1T-containing analogue **N(Ph-1T-DCN-Me)$_3$**. Glass transition temperatures for the whole series of compounds investigated tends to increase with increasing the conjugation length of the molecule, but decrease with increasing the alkyl chain length, albeit appearance of methyl group increase it as compared to the non-alkyl analogue. This tendency is reverse to the solubility trends discussed above. Heat capacity changes at the glass transition is quite close for all the compounds investigated and lies in the range of 0.21 – 0.29 J·g^{-1}K^{-1}.

X-ray diffraction measurements confirmed conclutions made form the DSC data. WAXS patterns of all three crystalline compounds – **N(Ph-1T-DCN-Me)$_3$**, **N(Ph-2T-DCN)$_3$**, and **N(Ph-2T-DCN-Me)$_3$** – reveal a number of narrow reflections, testifying unequivocally the presence of highly crystalline domains (Fig. 7a), while non-crystalline compounds showed only diffuse halo (Fig. 7b). Crystal packing of the molecules of compound **N(Ph-1T-DCN-Me)$_3$** were recently resolved.[26c] It forms triclinic crystal lattice with parameters a = 11.47 Å, b = 18.17 Å, c = 18.30 Å, α = 98.3°, β = 52.2°, γ = 130.7° (Fig. 8a). Similar crystal packing can be expected for the other two crystalline stars-shaped molecules, however their crystal lattice is not yet resolved. Temperature behaviour of **N(Ph-2T-DCN)$_3$** is presented on Fig. 9a. Glass transition manifests itself in the disappearance of the first of two diffuse halos and in the growth of a new reflection at s = 0.227 nm^{-1}.

Star-shaped compound with the longest alkyl group **N(Ph-2T-DCN-Dodec)$_3$** showed changed shape of the amorphous halo as compared to the other disordered compounds on Fig. 7b. Moreover, its SAXS patterns are characterized by a wide small-angle reflection corresponding to d-spacing of 30.3 Å (Fig. 9b, curves 1-3). With increasing temperature, mesophase reflection of this compound shifts to wider angles, d-spacing was being decreased to 29.5 Å at 60°C. Such change corresponds to thermal expansion coefficient $\beta = 6.6 \cdot 10^{-4}$ K^{-1} which is rather common for liquid crystalline materials and is due to shrinking of alkyl end chains. With increasing temperature a transition to isotropic phase is observed near 100°C. Mesophase order has not restored on cooling. Unfortunately structural data is not enough for unambiguous identification of the mesophase formed in as-received samples of compound **N(Ph-2T-DCN-Dodec)$_3$**. However some remarks could be made. According to the results of molecular modeling, the radius of molecular disc of **N(Ph-2T-DCN-Dodec)$_3$** is 26.5 Å provided the alkyl chains are in extended conformation, which coincides with great precise with diameter of columns if calculated from small-angle reflection d-spacing observed. Such supramolecular aggregate formed by twelve molecules is shown on Fig. 8b. Their arms are shifted relatively to each other by several degrees providing π–π stacking between neighboring arms of different molecules forming helical aggregate. However, as wide reflections as well as higher orders of 10 columnar reflection are not observed, such interpretation is open for further studies.

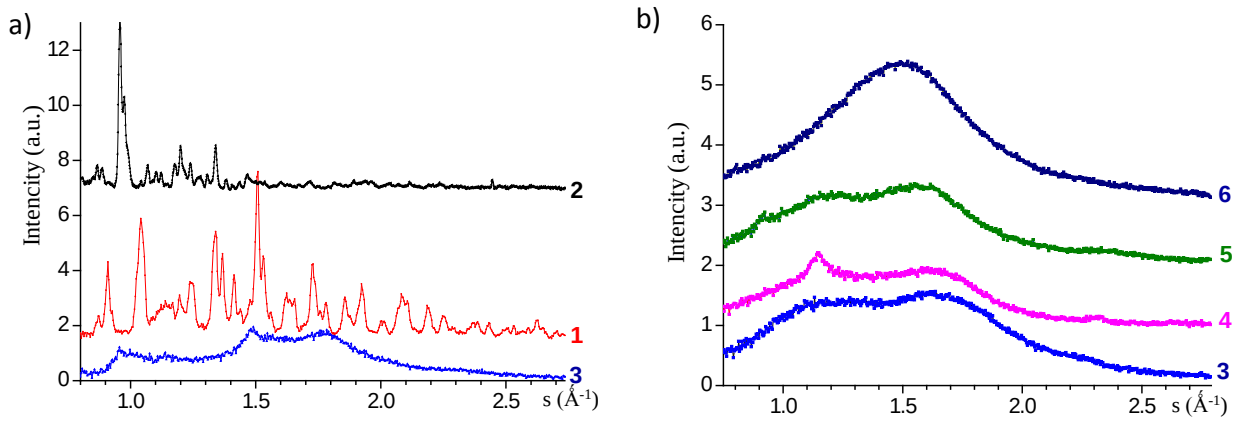

Fig. 7. WAXS patterns of (a) crystalline samples of 1) **N(Ph-2T-DCN)$_3$**, 2) **N(Ph-1T-DCN-Me)$_3$** and 3) crystalline fraction of **N(Ph-2T-DCN-Me)$_3$** and (b) amorphous samples of 3) **N(Ph-2T-DCN-Me)$_3$**, 4) **N(Ph-2T-DCN-Et)$_3$**, 5) **N(Ph-2T-DCN-Hex)$_3$**, 6) **N(Ph-2T-DCN-Dodec)$_3$**. For the sake of simplicity, scans are shifted along Intensity axis.For the sake of simplicity, scans are shifted along Intensity axis.

In contrast to the crystalline **N(Ph-2T-DCN)$_3$**, and to the amorphous **N(Ph-2T-DCN-Hex)$_3$**, which does not reveal any reflections in SAXS patterns (Fig. 9c, curve 1), **N(Ph-3T-DCN-Hex)$_3$** at room temperature is characterized by a set of three reflections with the ratios of corresponding d-spacings $d_1^2 : d_2^2 : d_3^2 = 1 : 3 : 4$ (Fig. 9c, curve 2). They can be indexed by 2D hexagonal columnar phase with cylinder diameter D = 23.7 Å. Moreover, wide halo is observed at s = 0.16 Å^{-1}. Its origin relates to

the Fourier transform of single cylinder of columnar mesophase. With the temperature increasing, mesophase reflections of compound **N(Ph-3T-DCN-Hex)$_3$** shift to small angles, diameter of the columns increased to 23.9 Å at 120°C (Fig. 9c, curve 3). Such a change corresponds to thermal expansion coefficient $\beta = 1.3 \cdot 10^{-4}$ K^{-1}. As the diameter of the molecule envelope is 30.6 Å, substantial correlation between the relative positions of the molecules in neighbouring molecules should be suggested (Fig. 8c). There is no order in the packing of the molecules along the column axis (because of the absence of diffraction maxima on wide-angle X-Ray scattering patterns), as well as no ordering between the neighbouring columns, summarizing the pattern of molecular packing is irregular in each transverse section due to the steric necessity of mutual packing of long π-conjugated bridges, while column centres form 2D hexagonal lattice. Appearing steric limitations lead to the azimuthal irregularities in stacking of the molecules along the column, as every molecule should adjust its position not only with its top and bottom neighbours inside the cylinder, but with its side neighbours as well. The columnar mesophase formed in the samples of **N(Ph-3T-DCN-Hex)$_3$** looks to be very promising for the directed charge transport along the columns as the oligothiophene fragments of neighbouring molecules are arranged to allow the best π–π stacking. However, an alignment of the columns is needed for the good semiconductor properties to manifest their selves.

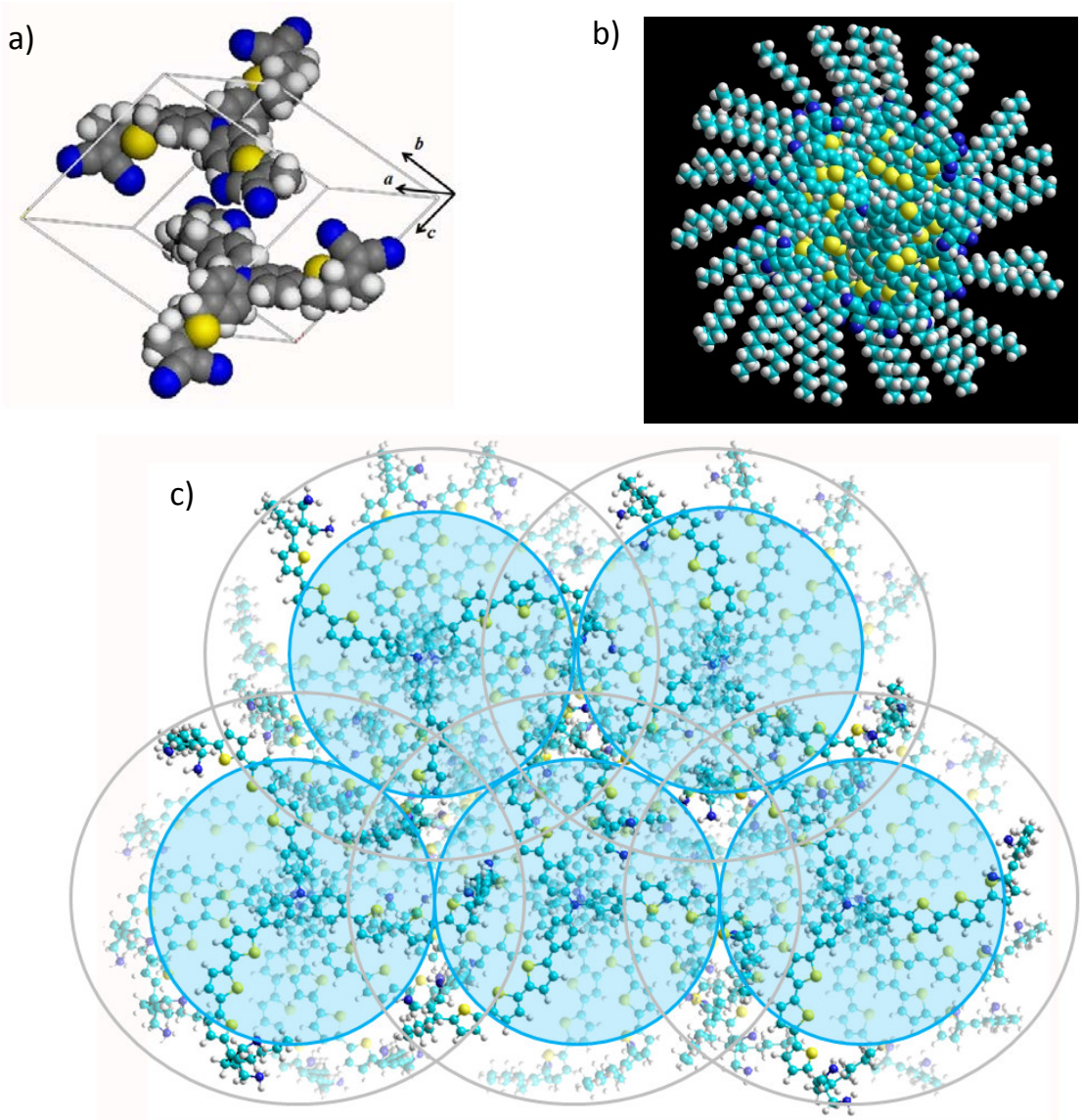

Fig. 8. (a) Packing of the molecules of compound **N(Ph-1T-DCN-Me)$_3$** in the triclinic crystal lattice with parameters a = 11.47 Å, b = 18.17 Å, c = 18.30 Å, α = 98.3°, β = 52.2°, γ = 130.7°. (b) Molecular modelling of the column formed by **N(Ph-2T-DCN-Dodec)$_3$** at low temperatures. (c) Molecular modelling of the packing of **N(Ph-3T-DCN-Hex)$_3$** molecules in 2D hexagonal columnar mesophase. Black solid circles correspond to 2D hexagonal columnar packing with the diameter of cylinders D = 23.7Å. Grey solid are the envelopes of molecular discs (D_m = 30.6 Å).

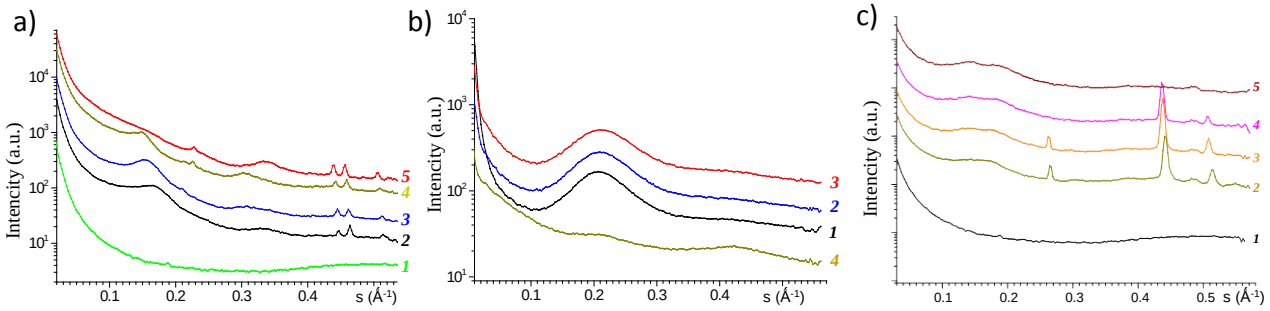

Fig. 9. SAXS patterns of (a) amorphous **N(Ph-2T-DCN-Me)$_3$** (1) and partially crystalline **N(Ph-2T-DCN)$_3$** (2-5) at room temperature (2), 100°C (3), 180°C (4), 250°C (5); (b) forming columnar mesophase **N(Ph-2T-DCN-Dodec)$_3$** at room temperature (1, as-received), 40°C (2), 60°C (3), and at room temperature after heating to isotropic phase (4); (c) amorphous **N(Ph-2T-DCN-Me)$_3$** (1) and forming hexagonal columnar mesophase **N(Ph-3T-DCN-Hex)$_3$** (2-5) at room temperature (2), 120 °C (3), 140°C (4), 160°C (5). For the sake of simplicity, scans are shifted along Intensity axis.

Thus, one can observe the tendency of the star-shaped compounds with short arms and short aliphatic tails to form crystalline structures. Moreover, it was shown before[29] that for the compound to form liquid crystalline mesophase, optimal combination of the rigid core and soft side chains should exist, which is the case for **N(Ph-2T-DCN-Dodec)$_3$** and **N(Ph-3T-DCN-Hex)$_3$**, but not the case for **N(Ph-2T-DCN-Me)$_3$**, **N(Ph-3T-DCN-Et)$_3$** or **N(Ph-2T-DCN-Hex)$_3$.**

Photovoltaic properties of star-shaped molecules with triphenylamine donor core and dicyanovinyl acceptor arms.

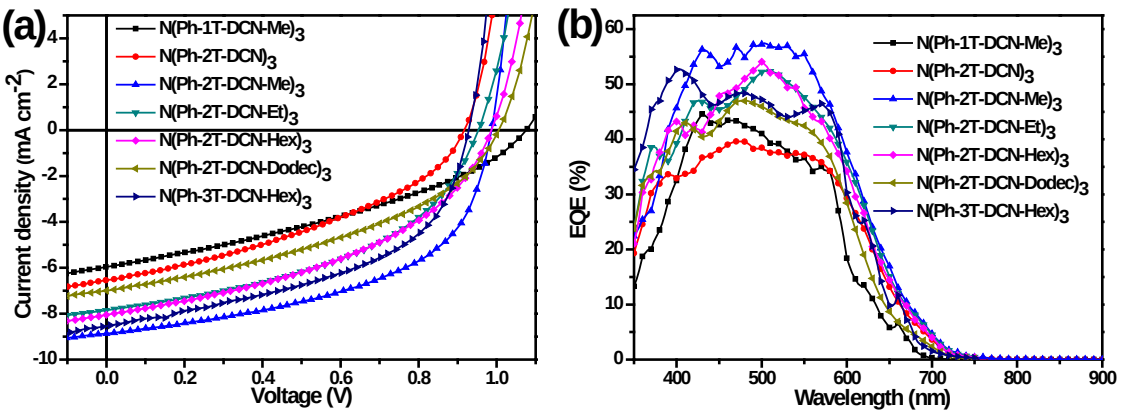

Fig. 10. Current density-voltage (*I-V*) curves (a) and EQE spectra (b) of solar cells based on **N(Ph-1T-DCN-Me)$_3$**:$PC_{70}BM$, **N(Ph-2T-DCN)$_3$**:$PC_{70}BM$, **N(Ph-2T-DCN-Me)$_3$**:$PC_{70}BM$, **N(Ph-2T-DCN-Et)$_3$**:$PC_{70}BM$, **N(Ph-2T-DCN-Hex)$_3$**:$PC_{70}BM$, **N(Ph-2T-DCN-Dodec)$_3$**:$PC_{70}BM$, and **N(Ph-3T-DCN-Hex)$_3$**:$PC_{70}BM$ (1:2, wt%), respectively, under the illumination of AM 1.5, 100 mWcm^{-2}.

To study the effects of oligothiophene π-bridge length as well as alkyl terminal chain length on the photovoltaic properties of star-shaped molecules, bulk heterojucntion organic solar cells (OSCs) with a configuration of ITO/PEDOT:PSS/TPA-based molecules: $PC_{70}BM$ (1:2, wt%)/Ca(15nm)/Ag(100nm) were fabricated. The best current density-voltage (*J-V*) curves are shown in Fig. 10a and the corresponding photovoltaic performance is summarized in Table 6. As expected, OSCs based on these small molecules show relatively high V_{oc} (>0.9 V), due to their low-lying HOMO energy levels. Encouragingly, OSC based on **N(Ph-1T-DCN-Me)$_3$** with thiophene bridges exhibited a high V_{oc} up to 1.08 V. In contrast, OSCs based on **N(Ph-3T-DCN-Hex)$_3$** with terthiophene bridges showed the lower V_{oc} of 0.93 V, which are consistent with their HOMO level variations. In addition, the other four 2T-bridge based molecules with various alkyl terminal chains exhibited the expected V_{oc} of 0.98 V, as shown in Table 6. However, the device based on **N(Ph-2T-DCN)$_3$** without alkyl terminal chains showed a low V_{oc} of 0.92 V, which may be attributed to poor film quality. Following this reasoning, a significant low J_{sc} of 6.54 mA cm^{-2} and a fill factor (FF) of 38.4% are observed for the **N(Ph-2T-DCN)$_3$**:$PC_{70}BM$ device. In these seven molecule systems, the **N(Ph-2T-DCN-Et)$_3$**:$PC_{70}BM$ device exhibited the highest power conversion efficiency (PCE) of 4.72% with a V_{oc} of

0.98 V, a J_{sc} of 8.87 mA cm^{-2}, and a FF of 54.3% under 100 mW cm^{-2} AM 1.5 G illumination. With the increasing of alkyl terminal chain length, the photovoltaic performance of relevant 2T-bridge based systems gradually decreased, as shown in Table 6. These results suggests that introduction of methyl terminal chains instead of the relatively long alkyl chains can enhance the intermolecular interactions, charge separation and transportation, charge carrier lifetime and consequently improving the photovoltaic performance. However, despite the device based on **N(Ph-1T-DCN-Me)$_3$** with thiophene bridges exhibited a high V_{oc} of 1.08 V, the J_{sc} (5.97 mA cm^{-2}) and FF (35.6%) of device significant drop due to the poor film quality and charge transport. In addition, compared to the **N(Ph-2T-DCN-Hex)$_3$**:$PC_{70}BM$ device, the **N(Ph-3T-DCN-Hex)$_3$**:$PC_{70}BM$ device showed the higher PCE of 3.96% with a slightly low V_{oc} of 0.93 V. It suggests that subtle extending π-bridge length in star-shaped molecules can represent an interesting toll for the effective modulation of the device performance at a moderate cost. The external quantum efficiency (EQE) of the corresponding devices is shown in Fig. 10b. And the integrated EQE agrees well with the J_{sc} of the various devices mentioned above.

Table 6. Photovoltaic properties of star-shaped molecules : $PC_{71}BM$ (1:2, wt%) devices, under the illumination of AM 1.5, 100 mW/cm^2.

Donor: $PC_{71}BM$	$V_{oc,}$ V	$J_{sc,}$ mA·cm^{-2}	FF, %	PCE, %
N(Ph-1T-DCN-Me)$_3$	1.08	5.97	35.6	2.30
N(Ph-2T-DCN)$_3$	0.92	6.54	38.4	2.31
N(Ph-2T-DCN-Me)$_3$	0.98	8.87	54.3	4.72
N(Ph-2T-DCN-Et)$_3$	0.96	7.86	46.0	3.47
N(Ph-2T-DCN-Hex)$_3$	0.98	8.07	43.1	3.41
N(Ph-2T-DCN-Dodec)$_3$	1.00	7.00	41.0	2.87
N(Ph-3T-DCN-Hex)$_3$	0.93	8.51	50.0	3.96

Experimental

General

^{1}H NMR spectra were recorded at a "Bruker WP-250 SY "spectrometer, working at a frequency of 250.13 MHz and utilising $CDCl_3$ signal (7.25 ppm) as the internal standard. In the case of 1H NMR spectroscopy, the compounds to be analysed were taken in the form of 5% solutions in $CDCl_3$. The spectra were then processed on the computer using the ACD Labs software.

Mass-spectra (MALDI) were registered on the Autoflex II Bruker (resolution FWHM 18000), equipped with nitrogen laser (work wavelength 337 nm and time-of-flight mass-detector working in reflections mode. The accelerating voltage was 20 kV. Samples were applied to a polished stainless steel substrate. Spectrum was recorded in the positive ion mode. The resulting spectrum was the sum of 300 spectra obtained at different points of sample. 2,5-dihydroxybenzoic acid (DHB) (Acros, 99%) and *α*-cyano-4-hydroxycinnamic acid (HCCA) (Acros, 99%) were used as matrices.

Elemental analysis of C, H, N elements was carried out using CHN automatic analyzer CE 1106 (Italy). The settling titration using BaCl2 was applied to analyze sulphur. Spectrophotometry technique was used for the Si analysis. Experimental error for elemental analysis is 0.30-0.50%. Experimental error is 0.30-0.50%. The Knövenagel condensation was carried out in the microwave "Discovery", (CEM corporation, USA), using a standard method with the open vessel option, 50 watts.

Thermogravimetric analysis was carried out in dynamic mode in 30 ÷ 900°C interval using Mettler Toledo TG50 system equipped with M3 microbalance allowing measuring the weight of samples in 0 - 150 mg range with 1 μg precision. Heating/cooling rate was chosen to be 10 °C/min. Every compound was studied twice: in air and in nitrogen flow of 200 ml/min. DSC scans were obtained with *Mettler Toledo DSC30* system with 10°C/min heating/cooling rate in temperature range of +20 - +290°C. Nitrogen flow of 50 ml/min was used.

Absorption profiles were recorded with a Perkin Elmer Lambda-35 absorption spectrometer from 350 to 1100 nm. Electrochemical properties were studied by cyclic voltammetry (CVA). The measurements were carried out in the 1,2-dichlorobenzene: acetonitrile (4:1) mixture of solvents using 0.1 M Bu_4NPF_6 as supporting electrolyte. The glassy carbon electrode was used as a work electrode. Potentials were measured relative to a saturated calomel electrode.

X-Ray diffraction. X-Ray diffraction patterns in small and wide angle scattering regions were recorded by S3-Micropix system (*Hecus* company), CuK_α-radiation, λ = 1.5406 Å with *Xenocs Genix* source (voltage and current - 50 kV and 1 mA respectively). *Pilatus* 100K detector was employed, as well as linear PSD 50M gas detector (Ar/Me mixture at $8•10^5$ Pa). Collimation system *Fox* 3D with Kratky

collimation slits of 0.1 mm and 0.2 mm width was used, allowing the stable measurements in wave vector range from s = 0.003 $Å^{-1}$ to s = 1.9 $Å^{-1}$ where s = $4\pi\sin\theta/\lambda$, 2θ is scattering angle. To get rid of the scattering of X Rays on air molecules, Goebbel mirrors and scattering path are vacuumed at pressures 2.6 ÷ 5.0 Pa. Exposure times were from 600 to 5000 s providing the high reliability of scattering data. Temperature behavior of samples was studied using Joule attachment in temperature range of 23˚C 300˚C. Transmission X-Ray diffraction patterns at wide angles were also recorded at *Bruker* D8 *Advance* powder diffractometer (CuK_α-radiation, λ = 1.5406 Å, Vantec 2D detector). *Accelrys Materials Studio*® program set was employed for molecular modeling of compounds studied. We used two sets of potentials, which allow taking into account non-covalent interactions: COMPASS (Condensed-phase Optimized Molecular Potentials for Atomistic Simulation Studies) and UFF (Universal Force Field). The COMPASS set is suitable for modeling of isolated molecules and condensed phases of mainly organic, polymeric and of some inorganic compounds,[H. Sun, J. Phys. Chem. B. 1998, 102, 7338-7364. H. Sun, Comput. Theor. Polym. Sci., 1998, 8, 229-246. D. Rigby, H. Sun, B. E. Eichinger, Polym. Int. 1998, 44, 311-330.] it also allows to parametrize partial charges and valency *ab initio* with subsequent system optimization.

Fabrication and characterization of the OSCs: All the devices were fabricated in the normal architecture. Photovoltaic devices were fabricated by doctor-blading on indium tin oxide (ITO)-covered glass substrates (from Osram). These substrates were cleaned in toluene, water, acetone, and isopropyl alcohol. After drying, the substrates were bladed with 50 nm PEDOT:PSS (HC Starck, PEDOT PH-4083). Photovoltaic layers, consisting of three different small molecules and $PC_{71}BM$ in 1:2 wt.% ratios were dissolved at different concentrations in ODCB and bladed on top of PEDOT:PSS layer. Finally, a calcium/silver top electrode of 15/80 nm thickness was evaporated. The typical active area of the investigated devices was 10.4 mm^2. The current-voltage characteristics of the solar cells were measured under AM1.5G irradiation on an OrielSol 1A Solar simulator (100 mW/cm^2). The EQE was detected with cary 500 Scan UV-Vis-NIR Spectrophotometer under monochromatic illumination, which was calibrated with a mono-crystalline silicon diode. Absorption profiles were recorded with a Perkin Elmer Lambda-35 absorption spectrometer from 350 to 1100 nm.

Materials

Tetrakis(triphenylphosphine)palladium(0)$Pd(PPh_3)_4$, magnesium, malononitrile, phosphorus(V) oxychloride, isopropoxy-4,4,5,5-tetramethyl-1,3,2-dioxaborolane (IPTMDOB), *tris*(4-bromophenyl)amine were obtained from Sigma–Aldrich Co. and used without further purification. 1,2-dichloroethane, THF, DMF, pyridine were dried and purified according to the known techniques and then used as solvents.

Synthesis

N(Ph-1T-DCN-Me)$_3$, **N(Ph-2T-DCN-Me)$_3$**, **N(Ph-2T-DCN-Et)$_3$**, **N(Ph-2T-DCN-Hex)$_3$**, **N(Ph-2T-DCN-Dec)$_3$** and **N(Ph-2T-DCN-Hex)$_3$** were synthesized as described elsewhere.[26]

2-(2,2'-bithien-5-yl)-4,4,5,5-tetramethyl-1,3,2-dioxaborolane (26). A solution of 5-bromo-2,2'-bithiophene (2.2 g, 9 mmol) in 22 mL of THF was added dropwise to a suspension of magnesium (0.27 g, 9.4 mmol) in 2 mL of THF. The Grignard reagent was refluxed for 2 h, then cooled to room temperature and 2-isopropoxy-4,4,5,5-tetramethyl-1,3,2-dioxaborolane (1.67 g, 9 mmol) was added in one portion. The reaction mixture was stirred for 1 h at room temperature, followed by stirring for 1 h at 40°C. After completion of the reaction 75 mL of freshly distilled diethyl ether and 100 mL of distilled water and 9 mL of 1M HCl were added to the reaction mixture. The organic phase was separated, washed with water, and dried over sodium sulfate and filtered. The solvent was evaporated to give 2.47 g (95%) of the product (purity was also 99% according to GPC and ^{1}H NMR) as a blue oil. The product was used in the subsequent synthesis without further purification. ^{1}H NMR (250 MHz, $CDCl_3$): 1.34 (s, 12H), 6.98–7.04 (m, 1H, M=4, *J* = 9.1 Hz), 7.21 (m, 3H, M = 4, J = 6.1 Hz), 7.51 (d, 1H, *J* = 3.7 Hz). Calcd (%) for $C_{14}H_{17}BO_2S_2$: C, 57.54; H, 5.86; S, 21.94. Found: C, 56.91; H, 5.72; S, 21.83. MALDI-MS: found m/z 292.59; calculated for $[M]^+$ 292.07.

***Tris*[4-(2,2'-bithien-5-yl)phenyl]amine (27)**. In an inert atmosphere, degassed solutions of tris(4-bromophenyl)amine (1.08 g, 2.24 mmol) and 2-(2,2'-bithien-5-yl)-4,4,5,5-tetramethyl-1,3,2-dioxaborolane (**1**) (2.36 g, 8.07 mmol) in toluene/ethanol mixture (40/4 mL) and 2M solution of aq. Na_2CO_3 (12.1 mL) were added to $Pd(PPh_3)_4$ (280 mg, 0.24 mmol). The reaction mixture was stirred under reflux for 9 h, and then it was cooled to room temperature and the organic phase was separated and the solvent was evaporated in vacuum and the residue was dried at 1 Torr. The product was passed through silica gel column (eluent hot toluene, 70 ºC) and recrystallized from toluene to give pure compound **2** (1.48 g, 90%) as a yellow solid. M.p.: 209-210 ºC. ^{1}H NMR (250 MHz, $CDCl_3$): δ [ppm] 7.01 (dd, 3H, J_1 = 3.7 Hz, J_2= 3.7 Hz), 7.12 (d, 6H, *J* = 4.3 Hz), 7.14–7.23 (overlapping peaks, 12H), 7.49 (d, 3H, *J* = 8.7 Hz). Calcd (%) for $C_{42}H_{27}NS_6$: C, 68.35; H, 3.69; N, 1.90; S, 26.07. Found: C, 67.88; H, 3.77; N, 1.82; S, 26.03. MALDI-MS: found m/z 735.45; calculated for $[M]^+$ 737.04

***Tris*[4-(5-formyl-2,2'-bithiophen-5-yl)phenyl]amine (28)**. *tris*[4-(2,2'-bithien-5-yl)phenyl]amine (**2**) (760 mg, 1.03 mmol) is dissolved in 50 mL of 1,2-dichloroethane. DMF (753 mg, 10.3 mmol) and $POCl_3$ (1579 mg, 10.3 mmol) are added dropwise and the mixture is refluxed 13 h under nitrogen. After cooling to room temp and addition of 50 mL of dichloromethane and 150 mL of a saturated aqueous solution of

sodium acetate, the mixture is stirred 2 h at room temperature. The organic phase is then washed with water and the organic phase was separated and the solvent was evaporated in vacuum and the residue was dried at 1 Torr. The product was recrystallized from toluene to give 760 mg (90%) of an orange solid. M.p.: 145-146 ºC. ^{1}H NMR (250 MHz, $CDCl_3$): δ [ppm] 7.14 (d, 6H, *J* = 8.7 Hz), 7.21 (d, 3H, *J* = 3.7 Hz), 7.32 (d, 3H, *J* = 4.3 Hz), 7.51 (d, 3H, *J* = 8.7 Hz), 7.66 (d, 6H, *J* = 4.3 Hz), 9.85 (s, 3H). IR (KBr) ν (cm^{-1}) : 1660 (C=O). Calcd (%) for $C_{45}H_{27}NS_6$: C, 65.75; H, 3.31; N, 1.70; S, 23.40. Found: C, 65.88; H, 3.27; N, 1.66; S, 23.30. MALDI-MS: found m/z 820.25; calculated for $[M]^+$ 821.03

2,2',2''-[nitrilotris(4,1-phenylene-2,2'-bithiene-5',5-diylmethylylidene)]trimalononitrile (N(Ph-2T-DCN)$_3$). Compound **3** (690 mg, 0.8 mmol), malononitrile (273.2 mg, 4.1 mmol) and dry pyridine (15 mL) were placed in a reaction vessel and stirred under argon atmosphere for 7 hours at 90 ºC using the microwave heating. After completeness of the reaction the pyridine was evaporated in vacuum and the residue was dried at 1 Torr. This crude product was purified by preparative GPC chromatography. Further purification included precipitation of the product from its THF solution with toluene and hexane to give pure product as a black solid (480 mg, 60%). ^{1}H NMR (250 MHz, DMSO-d6): δ [ppm] 7.06 (d, 6H, *J* = 3.7 Hz), 7.52 (d, 3H, *J* = 3.7 Hz), 7.58 (d, 3H, J = 3.7 Hz), 7.65 (m, 9H, M = 3, *J* = 7.9 Hz), 7.85 (d, 3H, *J* = 3.7 Hz), 8.59 (s, 3H). IR (KBr) ν (cm^{-1}) : 2220 (C≡N). Calcd. (%) for $C_{54}H_{27}N_7S_6$: C, 67.13; H, 2.82; N, 10.15; S, 19.91. Found: C, 66.98; H, 3.09; N, 9.78; S, 19.78. MALDI-MS: found m/z 963.41; calculated for $[M]^+$ 965.06.

Conclusions and outlook

Star-shaped oligomers present an emerging class of small molecules for efficient solution-procesible organic photovoltaics. The most prospective approach for design of such molecules is based on the "weak donor – strong acceptor" concept, similar to those used in the synthesis of low band gap copolymers.[15] In the case of star-shaped molecules the most successful weak donor is triphenylamine, which serves also as a convenient branching centre. Successful strong acceptors include benzo[1,2,5]thiadiazol and dicyanovinyl groups, which can be attached to the triphenylamine core either directly or via conjugated spacers from 2,5-thiphene or 1,2-vinylene units or their combination. Dicyanovinyl (DCN) groups seems to be more synthetically viable, however, typically they contain a liable imide proton -HC=C(DCN), originating from the aldehyde precursors, which can be easily oxidized. To avoid this drawback, we have developed a convenient synthetic approach, which allow using ketone precursor in the Knövenagel condensation, to form stable alkyl derivatives of dicyanovinyl groups.

Thus, alkyl groups, used also for increasing solubility of the small molecules, can influence their stability, morphology and structure in the bulk. It was found that adding methyl groups to dicyanovinyl acceptor units of the TPA-based star-shaped molecules decrease their melting points, but increase their melting enthalpy. These findings indicate that methyl end-capped molecules have stronger interactions in the bulks, leading to improved charge carrier mobilities and better photovoltaic performance. Comparison of **N(Ph-2T-DCN-Me)$_3$** and **N(Ph-2T-DCN)$_3$** shows that the presence of methyl groups in the molecule can lead to more than 2 times increasing in PCE: from 2.31 to 4.76%, when BHJ OSC were made under identical conditions. Such a strong effect is a result of improving of all the parameters influencing the PCE: open circuit voltage increases from 0.92 to 0.98V, short circuit current – from 6.54 to 8.87 mA/cm^2, and fill factor – from 38.4 to 54.3%. Enlarging the open circuit voltage can be related to lowering the HOMO energy level of the donor star-shaped molecule by 0.15 eV – a side effect of the improved oxidation stability. Better short circuit current can be explained by higher crystallinity and hence improved charge carried mobility. Improving the fill factor can be related to a better morphology of the bulk heterojunction in the case of methyl end-capped molecules.

Increasing the alkyl chain length leads to supressing the crystallinity and lowering the glass transition temperatures of the molecules. This fact influences positively on their solubility, but decreases the short circuit current and fill factors in BHJ OSCs, thus lowering their overall PCE to 3.47 – 2.87%. Nevertheless, ethyl group in **N(Ph-2T-DCN-Et)$_3$** seems to be a good compromise between the crystallinity and the solubility. This star-shaped compound is soluble not only in the chlorinated solvents, like most conjugated oligomers and polymers, but also in more environmentally friendly solvents, like benzaldehyde, that allow preparation of BHJ OSCs from green solvents with PCE = 3.6%.[30a] Moreover, this compound shows good PCE values up to 3.9% in the inverted structures of BHJ OSCs, which are more stable under normal conditions as the standard ones.[30b] Finally, interface engineering of the devices based on this donor molecule and $PC_{71}BM$ acceptor allows improving their PCE up to 5.4%.[30c]

Further increasing the alkyl chain length lead to a very interesting effect – **N(Ph-2T-DCN-Dodec)$_3$** forms a columnar ordering of the molecules. If it were not long dielectric dodecyl groups, it would lead to a record high PCE. Even stronger ordering was observed for **N(Ph-3T-DCN-Hex)$_3$** molecules – they form 2D hexagonal columnar mesophase. This factor definitely influences the performance of BHJ OSC based on this molecule, for which PCE approaches 4%.

Further improvements in the efficiency of the BHJ OCS based on star-shaped molecules are foreseen due to design of more flattened TPA-DCN molecules capable to formation of ordered 2D hexagonal columnar mesophase, and ordering of these phases in the devices. In addition, improved interfaces in BHJ OSCs checked for **N(Ph-2T-DCN-Et)$_3$**[30c] could lead to even higher performance for its methyl analogue **N(Ph-2T-DCN-Me)$_3$**.

Acknowledgements

Authors would like to thank Dr. P.V. Dmitryakov (NBICS center of Kurchatov Institute, Moscow, Russia) for DSC and TGA measurements and S.M. Peregudova (Institute of Organoelement Compounds of RAS, Moscow, Russia) for CVA measurements. This work in the part of synthesis and characterization of the oligomers was carried out under financial support of Russian Science Foundation (grant 14-13-01380). Preparation and characterization of photovoltaic devices have been funded by the

Sonderforschungsbereich 953 “Synthetic Carbon Allotropes”, the “Solar Technologies go Hybrid (SolTech)”, and the China Scholarship Council (CSC).

Notes and references

[a] Enikolopov Institute of Synthetic Polymeric Materials of the Russian Academy of Sciences, Profsoyuznaya st. 70, Moscow 117393, Russia.
[b] Chemistry Department, Moscow State University, Leninskie Gory 1-3, Moscow 119991, Russia.
[c] Institute of Materials for Electronics and Energy Technology (I-MEET), Friedrich-Alexander-University Erlangen-Nuremberg, Martensstraße 7, 91058 Erlangen, Germany.

Electronic Supplementary Information (ESI) available: ^{1}H NMR spectra, TGA curves. See DOI: 10.1039/b000000x/

1 R. Søndergaard, M. Hösel, D. Angmo, T. T. Larsen-Olsen and F. C. Krebs, *Materials Today*, 2012, **15**, 36-49.
2 Y. G. Liang and L.P. Yu, *Polymer Reviews*, 2010, **50**, 454-473.
3 (a) A. Mishra and P. Bauerle, *Angew. Chem. Int. Ed.* 2012, **51**, 2020-2067; (b) J. Roncali, P Leriche and P. Blanchard, *Adv. Mater*., 2014, **26**, 3821-3838.
4 C. J. Brabec, N. S. Sariciftci and J. C. Hummelen, *Adv. Funct. Mater*. 2001, **11**, 15-26.
5 A. J. Heeger, *Adv. Mater*., 2014, **26**, 10-28.
6 J. Peet, A. J. Heeger and G. C. Bazan, *Acc. Chem. Res*, 2009, **42**, 1700-1708.
7 Y. Huang, E. J. Kramer, A. J. Heeger and G. C. Bazan, *Chem. Rev.*, 2014, published online (dx.doi.org/10.1021/cr400353v).
8 P.A. Troshin, D.K. Susarova, E.A. Khakina, A.A. Goryachev, O.V. Borshchev, S.A. Ponomarenko, V.F. Razumov and N.S. Sariciftci, *J. Mater. Chem*., 2012, **22**, 18433-18441.
9 (a) J. Peet, J. Y. Kim, N. E. Coates, W. L. Ma, D. Moses, A. J. Heeger and G. C. Bazan, *Nat. Mater*., 2007, **6**, 497-500; (b) T.-Y. Chu, J.P. Lu, S. Beaupre, Y.G. Zhang, J.-R. Pouliot, S. Wakim, J.Y. Zhou, M. Leclerc, Z. Li, J.F. Ding and Y. Tao, *Am. Chem. Soc.*, 2011, **133**, 4250–4253; (c) J. A. Love, I. Nagao, Y. Huang, M. Kuik, V. Gupta, C. J. Takacs, J. E. Coughlin, L. Qi, T.S. van der Poll, E. J. Kramer, A.J. Heeger, T.-Q. Nguyen and G.C. Bazan, *J. Am. Chem. Soc.*, 2014, 136, 3597-3606.
10 H.-C. Liao, C.-C. Ho, C.-Y. Chang, M.-H. Jao, S. B. Darling and W.-F. Su, *Materials Today*, 2013, **16**, 326-336.
11 H.-L. Yip and A. K.-Y. Jen, *Energy Environ. Sci.*, 2012, **5**, 5994-6011.
12 (a) M. C. Scharber, D. Muehlbacher, M. Koppe, P. Denk, C. Waldauf, A. J. Heeger, C. J. Brabec, *Adv. Mater.* 2006, **18**, 789-794; (b) G. Dennler, M. C. Scharber, T. Ameri, P. Denk, K. Forberich, C. Waldauf, C. J. Brabec, *Adv. Mater*. 2008, **20**, 579-583.
13 (a) Y.G. Liang, Z. Xu, J.B. Xia, S.-T. Tsai, Y. Wu, G. Li, C. Ray and L.P. Yu, *Adv. Mater.* 2010, **22**, 135–138; (b) H. J. Son, W. Wang, T. Xu, Y.G. Liang, Y. Wu, G. Li and L.P. Yu, *Am. Chem. Soc.*, 2011, **133**, 1885–1894; (c) J. Zhou, Y. Zuo, X. Wan, G. Long, Q. Zhang, W. Ni, Y. Liu, Z. Li, G. He, C. Li, B. Kan, M. Li and Y. Chen, *J. Am. Chem. Soc.*, 2013, 134, 8484-8487; (d) Z.A. Tan, S. S. Li, F. Z. Wang, D. P. Qian, J. Lin, J.H. Hou and Y.F. Li, *Sci. Rep.* 2014, **4**, 4691. DOI:10.1038/srep04691.
14 (a) J.B. You, L.T. Dou, K. Yoshimura, T. Kato, K. Ohya, T. Moriarty, K. Emery, C.-C. Chen, J. Gao, G. Li and Y. Yang, *Nat. Commun*. 2013, **4**, 1446, DOI: 10.1038/ncomms2411; (b) Y.S. Liu, C.-C. Chen, Z. Hong, J. Gao, Y. M. Yang, H. P. Zhou, L. Dou, G. Li and Y. Yang, *Sci. Rep.* 2013, **3**, 3356, DOI:10.1038/srep03356; (c) J.B. You, C.-C. Chen, Z. Hong, K. Yoshimura, K. Ohya, R. Xu, S.L. Ye, J. Gao, G. Li and Y. Yang, *Adv. Mater*., 2013, **25**, 3973–3978.
15 H.X. Zhou, L.Q. Yang and W. You, *Macromolecules* 2012, **45**, 607−632.
16 R. de Bettignies, Y. Nicolas, P. Blanchard, E. Levillain, J. M. Nunzi and J. Roncali, *Adv. Mater*., 2003, **15**, 1939-1943.
17 (a) S.A. Ponomarenko, E.A. Tatarinova, A.M. Muzafarov, S. Kirchmeyer, L. Brassat, A. Mourran, M. Moeller, S. Setayesh and D. de Leeuw, *Chem. Mater*., 2006, **18**, 4101-4108 (b) P.A. Troshin, S.A. Ponomarenko, Y.N. Luponosov, E.A. Khakina, M. Egginger, T. Meyer-Friedrichsen, A. Elschner, S.M. Peregudova, M.I. Buzin, V.F. Razumov, N.S. Sariciftci and A.M. Muzafarov, *Solar Energy Materials & Solar Cells*, 2010, **94**, 2064–2072; D.A. Ivanov, D.V. Anokhin, M. Defaux, A. Mourran, M. Möller, Y.N. Luponosov, O.V. Borshchev, A.V. Bakirov, M.A. Shcherbina, S.N. Chvalun, T. Meyer-Friedrichsen, A. Elschner, S. Kirchmeyer and S.A. Ponomarenko, *J. Phys. Chem. C*, 2012, **116**, 22727-22736.
18 S. Roquet, R. Bettignies, P. Leriche, J. Roncali, *J. Mater. Chem*., 2006, **16**, 3040–3045.
19 E.A. Kleimyuk, P.A. Troshin, E.A. Khakina, Y.N. Luponosov, Y.L. Moskvin, S.M. Peregudova, S.D. Babenko, T. Meyer-Friedrichsen and S.A. Ponomarenko, *Energy & Environmental Sci.*, 2010, **3**, 1941-1948.
20 Y.N. Luponosov, A.N. Solodukhin and S.A. Ponomarenko, *Polymer Science, Ser. C*, 2014, **56**, 105–135.
21 A. Cravino, S. Roquet, O. Aleveque, P. Leriche, P. Frere and J. Roncali, *Chem. Mater*., 2006, **18**, 2584-2590.
22 (a) S. Roquet, A. Cravino, P. Leriche, O. Aleveque, P. Frere and J. Roncali, *J. Am. Chem. Soc*., 2006, **128**, 3459-3466; (b) A. Cravino, S. Roquet, P. Leriche, O. Aleveque, P. Frere and J. Roncali, *Chem. Commun*., 2006, 1416-1418; (c) A. Cravino, P. Leriche, O. Aleveque, S. Roquet and J. Roncali, *Adv. Mater*., 2006, 18, 3033-3037; (d) E. Ripaud, Y. Olivier, P. Leriche, J. Cornil and J. Roncali, *J. Phys. Chem. B* **2011**, 115, 9379-9386.
23 J. Cremer and P. Bauerle, *J. Mater. Chem*. 2006, **16**, 874-884.
24 (a) J. Zhang, D. Deng, C. He, Y. He, M. Zhang, Z.G. Zhang, Z. Zhang and Y. Li, *Chem. Mater*., 2011, **23**, 817-822; (b) D. Deng, S.L. Shen, J. Zhang, C. He, Z.J. Zhang and Y.F. Li, *Organic Electronics*, 2012, **13**, 2546–2552.

25 (a) G.L. Wu, G.J. Zhao, C He, J. Zhang, Q.G. He, X.M. Chen, Y.F. Li, *Solar Energy Materials & Solar Cells*, 2009, **93**, 108-113; (b) J. Zhang, J.T. Yu, C. He, D. Deng, Z.-G. Zhang, M.J. Zhang, Z.B. Li, Y.F. Li, *Organic Electronics*, 2012, **13**, 166–172; (c) J. Zhang, Y. Yang, C. He, Y.J. He, G.J. Zhao and Y.F. Li, *Macromolecules*, 2009, **42**, 7619-7622; (d) C. He, Q.G. He, Y.P. Yi, G.L. Wu, F.L. Bai, Z.G. Shuai and Y.F. Li, *J. Mater. Chem*., 2008, **18**, 4085-4090; (e) J. Zhang, Y. Yang, C. He, D. Deng, Z.B. Li and Y.F. Li, *J. Phys. D: Appl. Phys.*, 2011, **44**, 475101; (f) Y. Yang, Y. Zhou, Q.G. He, C. He, C.H. Yang, F.L. Bai and Y.F. Li, *J. Phys. Chem. B*, 2009, **113**, 7745-7752; (g) H.X. Shang, H.J. Fan, Y. Liu, W.P. Hu, Y.F. Li and X.W. Zhan, *Adv. Mater*., 2011, **23**, 1554–1557.

26 (a) J. Min, Y.N. Luponosov, T. Ameri, A. Elschner, S.M. Peregudova, D. Baran, T. Heumuller, N. Li, F. Machui, S. Ponomarenko and C.J. Brabec, *Organic Electronics*, 2013, **14**, 219-229; (b) J. Min, Y.N, Luponosov, A. Gerl, M.S. Polinskaya, S.M. Peregudova, P.V. Dmitryakov, A.V. Bakirov, M.A. Shcherbina, S.N. Chvalun, S. Grigorian, N. Kaush-Busies, S.A. Ponomarenko, T. Ameri, C.J. Brabec, *Adv. Energy Mater*., 2014, **4**, 1301234; (c) J. Min, Y.N. Luponosov, D. Baran, S.N. Chvalun, M.A. Shcherbina, A.V. Bakirov, P.V. Dmitryakov, S.M. Peregudova, N. Kausch-Busies, S.A. Ponomarenko, T. Ameri, C.J. Brabec, *J. Mater. Chem. A*, 2014, accepted (DOI: 10.1039/C4TA01933D).

27 (a) S.A. Ponomarenko, S. Kirchmeyer, A. Elschner, N.M. Alpatova M. Halik, H. Klauk, U. Zschieschang and G. Schmid, *Chem. Mater*., 2006, **18**, 579-586; (b) S.A. Ponomarenko, N.N. Rasulova, Y.N. Luponosov, N.M. Surin, M.I. Buzin, I. Leshchiner, S.M. Peregudova and A.M. Muzfarov, *Macromolecules*, 2012, **45**, 2014-2024.

28 J. Roncali, *Macromol. Rapid Commun*. 2007, **28**, 1761-1775.

29 (a) C. Destrade, N.H. Tinh, H. Gasparoux, J. Malthete, A.M. Levelut, *Mol. Cryst. Liq. Cryst.*, 1981, **71**, 111-135; (b) C. Destrade, P. Foucher, H. Gasparoux, N.H. Tinh, A.M. Levelut, J. Malthete, *Mol. Cryst. Liq. Cryst*. 1984, **106**, 121-146.

30 (a) I. Burgués-Ceballos, F. Machui, J. Min, T. Ameri, M.M. Voigt, Y.N. Luponosov, S.A. Ponomarenko, P.D. Lacharmoise, M. Campoy-Quiles, C.J. Brabec. *Adv. Funct. Mater*. 2014, **24**, 1449-1457; (b) J. Min, H. Zhang, T. Stubhan, Y.N. Luponosov, M. Kraft, S.A. Ponomarenko, T. Ameri, U. Scherf, C.J. Brabec. *J. Mater. Chem. A*, 2013, **1**, 11306-11311; (c) J. Min, Y.N. Luponosov, Z.G. Zhang, S.A. Ponomarenko, T. Ameri, Y.F. Li and C.J. Brabec (submitted).

